HHS Public Access

Author manuscript

Nature. Author manuscript; available in PMC 2020 March 19.

Published in final edited form as:

Nature. 2019 July ; 571(7764): 198–204. doi:10.1038/s41586-019-1336-7.

Neural signatures of sleep in zebrafish

Louis C. Leung[1], **Gordon X. Wang**[1], **Romain Madelaine**[1], **Gemini Skariah**[1], **Koichi Kawakami**[2], **Karl Deisseroth**[3,4,5], **Alexander E. Urban**[6], **Philippe Mourrain**[1,7,*]

[1]Center for Sleep Sciences and Medicine, Department of Psychiatry and Behavioral Sciences, Stanford University, Stanford, CA, USA.

[2]Division of Molecular and Developmental Biology, National Institute of Genetics and Department of Genetics, Sokendai, Mishima, Japan.

[3]Howard Hughes Medical Institute, Stanford, CA, USA.

[4]Department of Bioengineering, Stanford University, Stanford, CA, USA.

[5]Department of Psychiatry and Behavioral Sciences, Stanford University, Stanford, CA, USA.

[6]Center for Genomics and Personalized Medicine, Department of Psychiatry and Behavioral Sciences, Stanford University, Stanford, CA, USA.

[7]INSERM 1024, Ecole Normale Supérieure, Paris, France.

Abstract

Slow-wave sleep and rapid eye movement (or paradoxical) sleep have been found in mammals, birds and lizards, but it is unclear whether these neuronal signatures are found in non-amniotic vertebrates. Here we develop non-invasive fluorescence-based polysomnography for zebrafish, and show—using unbiased, brain-wide activity recording coupled with assessment of eye movement, muscle dynamics and heart rate—that there are at least two major sleep signatures in zebrafish. These signatures, which we term slow bursting sleep and propagating wave sleep, share commonalities with those of slow-wave sleep and paradoxical or rapid eye movement sleep, respectively. Further, we find that melanin-concentrating hormone signalling (which is involved in

[*]**Correspondence and requests for materials** should be addressed to P.M., mourrain@stanford.edu.

Author contributions

L.C.L., G.X.W. and P.M. conceived the study. L.C.L. and P.M. designed experiments. L.C.L. and G.X.W. built the imaging platform and computing hardware. L.C.L., R.M., K.K. and G.S. performed cloning and generated transgenic lines and mutants. L.C.L. performed all experiments except for two-photon imaging (G.X.W.). L.C.L. and G.X.W. developed and wrote the computational pipeline. L.C.L. performed analysis and produced the figures. K.D. provided project mentorship. A.E.U. provided genome analysis and mentorship. L.C.L. and P.M. wrote the paper with contributions from all authors.

Online content

Any methods, additional references, Nature Research reporting summaries, source data, statements of data availability and associated accession codes are available at https://doi.org/10.1038/s41586-019-1336-7.

Reviewer information *Nature* thanks Herwig Baier and the other anonymous reviewer(s) for their contribution to the peer review of this work.

Competing interests The authors declare no competing interests.

Extended data is available for this paper at https://doi.org/10.1038/s41586-019-1336-7.

Supplementary information is available for this paper at https://doi.org/10.1038/s41586-019-1336-7.

mammalian sleep) also regulates propagating wave sleep signatures and the overall amount of sleep in zebrafish, probably via activation of ependymal cells. These observations suggest that common neural signatures of sleep may have emerged in the vertebrate brain over 450 million years ago.

Sleep has been described in all branches of the animal kingdom using behavioural criteria[1–3]. This sleep definition has been further expanded to include the main electrophysiological hallmarks of human sleep such as slow-wave sleep (SWS) and paradoxical or rapid eye movement (REM) sleep (abbreviated to PS/REM when referred to collectively), which so far have only been reported in mammals, birds and reptiles[1,2,4]. It is unclear whether these phenomena exist in non-amniotic vertebrates such as fishes and amphibians, which leaves open the question of whether these states are specific to recent evolution of the neocortex or whether they emerged along with the vertebrate brain over 450 million years ago[2] (Extended Data Fig. 1a).

In the diurnal vertebrate zebrafish, a bona fide sleep state has been well-established through behavioural criteria; both adult and larval zebrafish exhibit circadian-regulated periods of reversible immobility associated with an increased arousal threshold[5–7], as well as sleep rebound in response to sleep deprivation[6–9]. However, it is difficult to find neuronal sleep signatures in a fish brain because of the absence of a conventional neocortex, at which electroencephalograms (EEG) are typically recorded. Nevertheless, teleost fish possess the dorsal pallium (considered to be a homologue of the neocortex[10]), which suggests that sleep signatures might be found by examining this region. Crucially, the major sleep circuits and neuromodulators that are implicated in the regulation of the sleep–wake cycle (such as hypothalamic histamine, hypocretin and melanin-concentrating hormone (MCH), and pontine acetylcholine and GABA) are mostly found in the subcortex, and are well-conserved across vertebrate species from human to zebrafish[6,9,11] (Extended Data Fig. 1a), which raises the question of whether there are conserved subcortical signatures of sleep.

Neuronal activity in slow oscillating sleep

The compact size and linear rostrocaudal organization of the translucent brain of the larval zebrafish presents an opportunity to identify—in an agnostic fashion—the neuronal sleep signatures that could have pre-existed the radiation of amniotes. We therefore first recorded neuronal activity during sleep in the dorsal pallium of one-to two-week-old zebrafish larvae that expressed the calcium indicator GCaMP6F[12] under a panneuronal promoter[13] (Fig. 1a, b). To promote sleep under restraint and light-microscopy conditions, larvae underwent sleep deprivation (Extended Data Fig. 1b, Methods). Behavioural sleep was first assessed by actimetry to ensure optimal conditions for sleep consolidation (Extended Data Fig. 1c–e), as previously established[5,7,9]. After sleep deprivation, larvae were imaged at single-cell resolution for dorsal pallium activity, and compared to non-sleep-deprived sibling controls. We observed that in awake, non-sleep-deprived fish high spontaneous activity in the telencephalon occurred at the anterolateral regions of the dorsal pallium, and was desynchronous (Fig. 1c, e, see Supplementary Information, supplementary video 1). Notably, when asleep, sleep-deprived fish displayed highly synchronous bursts of activity

punctuated by periods of silence in the dorsal pallium (Fig. 1d, f, see Supplementary Information, supplementary video 2). Quantification of activity in each pallial hemisphere of sleep-deprived versus non-sleep-deprived brains showed significant shifts in three metrics of activity and synchronicity within and between hemispheres: periodicity (the inter Ca^{2+} transient interval (ITI)), amplitude and coherence index (coincident firing of >50% of a population per epoch (Methods, Supplementary Fig. 1)). During sleep, the average interval of firing activity was longer (sleep-deprived ITI of 12.26 ± 2.91 s versus non-sleep-deprived ITI of 3.84 ± 0.14 s) (Extended Data Fig. 1f), and—in sleep-deprived fish—the average burst intensity of Ca^{2+} transients was higher in sleep than those observed during wake (25.75 ± 0.29% increase in spike fluorescence) (Fig. 1d, f). The coherence index, which measures inter-neuronal synchronicity, was significantly higher for sleep-deprived brains compared to non-sleep-deprived ((18.84% versus 6.38%, respectively) (Fig. 1d, f). Further, the probability of observing the signature of what we here term slow bursting sleep (SBS) (synchronous ITI band of 5–30 s) increased with the duration of sleep deprivation (non-sleep-deprived 0%, 1-d sleep deprivation 25%, 2-d sleep deprivation 57% and 3-d sleep-deprivation 71%) (Extended Data Fig. 1g), which suggests that the occurrence of SBS activity in zebrafish is proportional to sleep pressure (sleep homeostasis).

Pallial sleep signatures with hypnotics

We next investigated whether sleep-related neuronal activities, such as the SBS signature, could be induced with hypnotic compounds. Stimulation of non-sleep-deprived fish with hypnotics at doses that induce behavioural sleep states (Supplementary Table 1) revealed three categories of neuronal signature in the dorsal pallium (Fig. 2b, c, Extended Data Fig. 2): SBS, broad silencing and waveforms that travel in a caudal-to-rostral direction (see Supplementary Information for description of dimensionality reduction in Fig. 2). Unlike carrier controls (Fig. 2a), intra- and inter-hemispheric SBS were induced by the histamine receptor (H1R) antagonists mepyramine (Fig. 2b, see Supplementary Information, supplementary video 3) and promethazine (Extended Data Fig. 2a). We found increased slow synchronous activity upon treatment with these compounds, as shown by changes in the ITI (4.42 ± 0.38 s versus 16.55 ± 6.79 s), amplitude (25.37% increase) and coherence index (6.06% versus 31.18%) between baseline and mepyramine dynamics. Similar to sleep deprivation, H1R antagonism in zebrafish increases neuronal network synchronicity, resulting in slower-frequency, higher-amplitude neuronal bursts in the dorsal pallium of sleeping fish; together, these observations reflect a state that shares commonalities with mammalian SWS. Indeed, EEG slow waves reflect the oscillation of synchronized on–off activity in cortical neurons[14]. Similar to the role of slow-wave activity as the primary indicator of the length of prior wakefulness or sleep pressure[15,16], we found that increases in SBS were proportional to the duration of sleep deprivation. Indeed, in rodents and cats, H1R antagonism specifically increases and consolidates SWS at the expense of REM sleep[17–19]. However, a notable difference between SBS dynamics and SWS is the relatively slower speed of the former (see Supplementary Information for discussion of the infra-slow band (<0.1 Hz)). Our data suggest that synchronous oscillatory neuronal states during sleep may have arisen earlier than previously expected in the evolution of the vertebrate nervous system.

Unlike SBS, the hypnotic $GABA_A$-receptor agonist gaboxadol and the anaesthetic MS222 induced sustained silencing in overall activity in the dorsal pallium (Extended Data Fig. 2b, c, see Supplementary Information, supplementary videos 4, 5). It has previously been reported in mice that a broad reduction in overall cortical activity occurs during sleep[20], which suggests that this reduction might be a feature of sleep and would be consistent with the hypnotic effect of gaboxadol in flies[21]. However, it is doubtful that such total, unbiased shutdown of firing represents a bona fide sleep state; the similarity between the states induced by gaboxadol and the MS222 anaesthetic therefore led us to reject this compound from further study.

The final category of sleep signature is characterized by travelling waves of neuronal activity that spread anteriorly across the telencephalon. This specific signature was induced by three compounds: the non-benzodiazepine imidazopyridine hypnotic zolpidem[22] (Extended Data Fig. 2d, see Supplementary Information, supplementary video 6), the cholinomimetic carbachol (Fig. 2c, see Supplementary Information, supplementary video 7) and eserine[23], an acetylcholine esterase inhibitor (Extended Data Fig. 2e). We observed a sequence of activations that started with a noticeable relaxation of the telencephalon (seen by tissue distention; see Supplementary Information, supplementary video 7), followed by a stereotyped caudal-to-rostral midline activation, and then by a high-amplitude wave (with a mean duration of about 2.5 min) that swept through the telencephalon (Fig. 2c). After this transient wave, there is a return to desynchronized activity in the dorsal pallium. Together, we find that—at the dorsal pallium—at least two neuronal sleep signatures are revealed at single-cell resolution: SBS and travelling waves.

Fluorescence-based polysomnography for SBS

As sleep is a body-wide phenomenon that cannot be defined solely by a telencephalic neuronal signature, we sought to incorporate a measure of the physiological parameters used to define sleep through polysomnography (PSG). We developed an imaging platform that combined a custom light-sheet microscope—which enables high-speed, wide-field and pixel-synchronous acquisition across the animal (Fig. 3a)—with a transgenic zebrafish line (which we named ‘zPSG’) that expresses GCaMP7a in the brain and trunk muscles and GFP in the heart (Fig. 3b, Methods) to perform fluorescence-based (f)PSG. fPSG recapitulates PSG in fish (Fig. 3c) through proxies for brain activity (an fEEG), muscle activity (a fluorescence-based electromyogram (fEMG)), heart rate (a fluorescence-based electrocardiogram (fECG)) and eye movement (a fluorescence-based electrooculogram (fEOG)).

Consistent with our telencephalic imaging, both sleep deprivation and treatment with antihistamines revealed intra- and inter-hemispheric synchronicity in the dorsal pallium during fPSG, along with broadly reduced ‘subcortical’ brain activity (Extended Data Fig. 3a–e, see Supplementary Information, supplementary video 13). Compared to the wake state, an associated decrease in Ca^{2+} transients in trunk muscle cells was observed during SBS, which is consistent with reduced actimetry during sleep (fEMG in Fig. 3d). Analysis of eye movement also showed a notable absence of saccades (fEOG in Fig. 3d). The heart rate decreased on average twofold, from about 200 beats per minute during wakefulness to about

120 beats per minute during sleep rebound or about 110 beats per minute upon treatment with mepyramine (fECG in Fig. 3d), and maintained a tight distribution of interbeat intervals (about 500–600 ms) (fECG in Fig. 3d, Extended Data Fig. 4).

To confirm that SBS also occurs during the normal circadian night, we implemented a wake-maintenance method to gently consolidate wake (and thus subsequent sleep) during daylight hours, before performing night-phase fPSG (Methods). Similar to sleep rebound and treatment with antihistamine, we observed SBS (as defined by fPSG) during the normal circadian night (Extended Data Figs. 9, 10). Finally, we found that habituation to agarose restraint of untreated larvae allowed spontaneous expression of SBS signatures during normal circadian night (Extended Data Fig. 11, Methods, see Supplementary Information, supplementary video 17). Together, fPSG experiments demonstrated that during sleep induced by hypnotics, sleep rebound, sleep after wake maintenance and spontaneous sleep, SBS is tightly associated with synchronous dorsal pallium activity and with reductions in muscle, eye and cardiorespiratory activity. These features confirm behavioural observations of sleep states in fish, and share polysomnographic commonalities with non-REM SWS in mammals, birds and reptiles.

fPSG for propagating wave sleep

Our data showed travelling waves that arrived from beyond the telencephalon, which prompted us to use fPSG to fully capture the generation of this sleep signature. Expanding our analysis to the whole-brain scale allowed us to uncover a rich fluid sequence that starts with a bilateral anteroposterior wave of muscular activation, midline and ventricular zone activation, followed by a travelling wave of neuronal activation that propagates rostrally from the pons to the telencephalon, as seen on treatment with carbachol (fEEG in Fig. 3e, Extended Data Fig. 3h; detailed staging is shown in Supplementary Information, supplementary videos 8, 9, 19), eserine (Extended Data Fig. 5b, see Supplementary Information, supplementary video 10) or zolpidem (Extended Data Fig. 5e, see Supplementary Information, supplementary video 11). Inductions of these activities with either carbachol or eserine were blocked by pre-incubation with methoctramine, an inhibitor of muscarinic acetylcholine receptors (M2 and M4) (Extended Data Fig. 5c, d), which confirmed the specific involvement of cholinergic neurotransmission. We refer to the brain wave dynamic that is common to cholinergic and GABAergic induction as the ponto-midbrain-telencephalic (PMT) wave.

While the fPSG initially recorded the normal awake profile that features frequent eye saccades, active muscle tone and a heart rate of about 200 beats per minute (with a regular interbeat interval of about 300 ms) (Fig. 3e, see Supplementary Information, supplementary videos 9, 16), the PMT wave marked the onset of a sleep state that we term propagating wave sleep (PWS) (Fig. 3e, Extended Data Fig. 3f–h), which has features that are consistent with previously recorded cholinergic and GABAergic-induced behavioural sleep. First, muscle activity showed a rapid and total loss of muscle tone, which persisted (fEMG in Fig. 3e). Second, spontaneous eye movements gave way to a slow roll (relaxation; black box in the fEOG panel of Fig. 3e) before stopping entirely. Third, the heart rate not only dropped to about 90 beats per minute but also showed increased variance in the distribution of interbeat

intervals (700–1,100 ms, coefficient of variation 0.13 versus 0.64) (fECG in Fig. 3e, Extended Data Fig. 4a, d). This PWS state is distinct from SBS, in which muscle tone decreased but was not absent and heart beat was slow but regular (coefficient of variation 0.18 versus 0.13) (Extended Data Fig. 4). Unlike in SBS (in which dorsal pallium neurons oscillate synchronously between on and off activity), desynchronous activity close to ITIs and coherence indices observed during the wake state is resumed after the PMT wave (pre-PMT wave versus post-PMT wave ITI 2.88 ± 2.14 s versus 2.96 ± 1.35 s; coherence index, 1.32% versus 1.08%) (Extended Data Fig. 3f, g).

As with SBS, we further sought to examine the presence of PMT waves and subsequent dynamics during daytime sleep rebound after sleep deprivation, during night-phase sleep after wake maintenance and after habituation of untreated larva. Confirming pharmacologically induced PMT signatures, we observed that, after sleep deprivation, there were rare instances of PWS dynamics that included extended periods of midline ventricular activation before the onset of PMT waves (see Supplementary Information, supplementary video 12). Finally, in normal night-phase sleep, we found spontaneous PMT waves that were associated with muscle atonia and wake-like active dorsal pallium (Extended Data Figs. 10, 11, Supplementary Fig. 2 and Supplementary Information, supplementary video 18).

PWS is reminiscent of PS/REM, with which it shares at least six commonalities—including pontine waveforms (PMT versus ponto-geniculo-occipital waves[24,25]), wake-like activity in dorsal pallium (equivalent to paradoxical activity in PS/REM), a total loss of muscle tone, increased variability in heart rate, induction by cholinergic or GABAergic agonists[23,26], and blockade by M2 and M4 antagonists[27,28]. One notable difference between PWS and REM is the absence of the hallmark rapid eye movements of the eponymous mammalian sleep state. This is consistent with the absence of rapid eye movements during adult zebrafish sleep, despite the fact that other physiological features of PS/REM (such as slow and irregular breathing) remain present[29]. Future studies in fishes and other non-mammalian vertebrates will uncover whether PWS is analogous to PS/REM.

Ependymal cells as precursors to sleep onset

Our unbiased, brain-wide activity screen provided an opportunity to find novel cell types that are potentially involved in sleep regulation. Notably, a motif that appeared robustly at the onset of the PWS activitome was the midline-cell activation that appeared to span the anteroposterior axis of the brain (panel h2 in Extended Data Fig. 3). We serendipitously identified a zebrafish line that expressed mCherry in cells that matched the characteristic ventricular location, triangular cell morphology and long thin processes of the activated cells (Extended Data Fig. 6b, c). By crossing this line with our zPSG line, we confirmed that a large subset of mCherry-positive cells were the same periventricular cell types that were activated before the PMT wave (Extended Data Fig. 6d–f) and subsequently inactivated as the wave continued through the brain (Extended Data Fig. 6f, g, Supplementary Information, supplementary video 14). On the basis of their positioning and morphology, and the fact that they were α-tubulin-positive and largely glial fibrillary acidic protein (GFAP)-negative at this developmental stage[30] (Extended Data Fig. 6b, c), we consider these cells to be specialized ependymal cells or perhaps tanycytes, which have known functions in

controlling the flow of cerebrospinal fluid[31–33]. The attempted physical removal of ependymal cells to examine their roles proved lethal, probably owing to the critical roles of these cells in maintaining periventricular tissue integrity (Extended Data Fig. 7; see Supplementary Information for detailed description). As sleep regulators such as hypocretin (also known as orexin), MCH, histamine and other neurotransmitters can signal through the cerebrospinal fluid (potentially via ependymal cells), we sought other methods to probe the functional role of ependymal cells in PWS dynamics in zebrafish.

Ependymal cells, MCH, pigments and sleep

A conserved property of ependymal cells is their activation by MCH, which is a well-known modulator of sleep[34] and skin pigmentation[35]. Ciliated ependymal cells express MCH[36] and MCHR1[31], and ex vivo experiments have shown the former can stimulate increased Ca^{2+} transients that upregulate ciliary beat frequency[31,37], which led us to ask whether MCH could directly activate zebrafish ependymal cells. To examine this, we injected MCH into the intracerebroventricular cavity of zPSG fish (Extended Data Fig. 7h). Significant increases in GCaMP fluorescence in periventricular cells in response to MCH, compared to mock- or carrier-injected fish (−0.98% versus +53.74% (Extended Data Fig. 6h–m), provides functional evidence for their identity as ependymal cells and their potential involvement in the MCH-dependent regulation of sleep. Consistent with the association between MCH and its pigmentation functions in fish, we uncovered a notable coupling of epidermal melanin spreading and contraction to ependymal cell activation and PMT waves (Extended Data Fig. 6, Supplementary Information for detailed description, Supplementary Information, supplementary video 15). This finding not only points to MCH as a key mediator in coregulating pigmentation and sleep dynamics in zebrafish, but also has implications for the many vertebrate species (including fishes, amphibians and reptiles) that adapt their coloration during sleep as cryptic or aposematic strategies to avoid predation.

In mammals, MCH neurons fire maximally during REM sleep[38]; optogenetic activation, as well as intracerebroventricular injection with MCH peptide, can promote REM[34,39]. MCH2 has previously been identified as the true homologue in fishes of mammalian MCH, as well as its receptors[11]. We therefore used three loss-of-function strategies to examine the role of MCH signalling in both regulating PWS signatures (ependymal cell activation and PMT waves) and the overall amount of behavioural sleep.

First, to test whether the removal of MCH2 neurons disrupted sleep brain signatures and behaviour, a fish line that expresses enhanced nitroreductase under the control of the MCH2 promoter was generated and crossed into the zPSG line (Extended Data Fig. 8a, b). Chemogenetic ablation was induced by incubation with metronidazole. When imaged in a two-hour incubation of carbachol, MCH2-neuron-ablated fish produced far fewer ependymal cell activations (100% versus 29%) or PMT waves (100% versus 21%) than sibling transgene-negative controls treated with metronidazole—and those activations that did occur were significantly delayed (Fig. 4a). In parallel, actimetry over an entire sleep–wake cycle of free-swimming MCH2-neuron-ablated transgenic fish revealed a twofold decrease in the amount of sleep during the night, as compared to treated sibling controls (Fig. 4b, c, Supplementary Table 2).

Second, we used the MCHR1 inhibitor H6408, which has previously been shown to prevent the MCH modulation of ciliary beat frequency in ependymal cells[37]. Pre-incubation of H6408 significantly affected the ability of carbachol to activate ependymal cells (100% versus 42%) and PMT waves (88.5% versus 42%) in zPSG fish (Extended Data Fig. 8k). In actimetry experiments, there was an initial marked increase in basal activity after a two-hour H6408 incubation, although this transient effect did not significantly affect long-term sleep patterning at these concentrations (Extended Data Fig. 8l, m, Supplementary Table 2).

Finally, for the constitutive disruption of MCHR signalling in zPSG fish, we generated double mutants against both subtypes of MCHR1 (MCHR1a and MCHR1b) using CRISPR–Cas9 and TILLING approaches, respectively (Fig. 4d–f). These MCHR1a MCHR1b double mutants exhibit significant disruption of ependymal cell activation (100% versus 50%) and induction of PMT waves (90% versus 16%), with a marked delay relative to non-mutants (Fig. 4d). Consistent with the disruption in their sleep neuronal signatures, the double-mutant (*mchr1a*$^{-/-}$*mchr1b*$^{-/-}$) zebrafish displayed increases in day and night activity with a significant reduction in the amount of sleep at night compared to non-mutants (*mchr1a*$^{+/+}$*mchr1b*$^{+/+}$) (Fig. 4e, f, Supplementary Table 2). These results show that MCH signalling has an important role in activating the PWS signature, and in regulating the amount of sleep, in zebrafish.

Discussion

Over a century ago, behavioural criteria were established that enabled the first scientific description of the sleep state in fishes[3]. Here we identify the first neuronal sleep signatures in teleost fishes: slow synchronous ON–OFF oscillations in the dorsal pallium (the SBS state) and a sleep state initiated with propagating waves (the PWS state), both of which occur in an overall background of reduced brain activity (see Supplementary Information for discussion of silencing as a signature). SBS and PWS dynamics share many commonalities with those of SWS and PS/REM, respectively, which suggests that sleep-related neuronal signatures coupled with characteristic muscular signatures (in heart, eye and voluntary muscle) may have emerged much earlier than the radiation of amniotes (about 450 million years ago), and that they probably mark ancestral sleep functions that are essential across vertebrates.

Using cellular-resolution polysomnography in zebrafish, we have identified the very first neural cells that are activated before PWS, and often before SBS: the periventricular ependymal cells. Ependymal cells express MCHR[37] and, as ciliated cells, participate in the flow of sleep-related neurotransmitters throughout the ventricular system of the brain (see Supplementary Information for discussion of potential roles of ependymal cells in sleep). We found that fish ependymal cells are activated by MCH; this neuropeptide is implicated in mammalian REM, but its role in sleep in fishes has been under debate since its discovery in salmon in 1983[40]. We show that disruption of the MCH signal perturbs PWS and greatly reduces sleep quantity, which suggests that it has a sleep-promoting role in fishes that is similar to its role in mammals (see Supplementary Information for discussion of the sleep role of MCH in fishes).

fPSG enables the non-invasive holistic capture of the choreography of physiological responses that are required for sleep–wake regulation. The agnostic identification of new sleep substrates paves the way for the investigation of cellular and molecular mechanisms that could potentially generate therapeutic targets. The power of fPSG could also be harnessed to profile hypnotics on the basis of not only the central nervous system activitome but also their cellular effect on organ systems that are optically accessible in the zebrafish, a platform that has the potential to be extended to model sleep disorders or other complex psychiatric behaviours.

METHODS

Zebrafish husbandry.

Zebrafish larvae were raised in E3 at 26 °C with a light cycle of 14-h day starting at 09:00 and 10-h night beginning at 23:00. Zebrafish were used at 7–14 days post-fertilization (dpf) in this study (see specifics in 'Behavioural assays, Sleep deprivation, Pharmacological reagents, Sample preparation and Ca2+ imaging and Cell ablation') were used in this study; the sex of the fish could not be determined at this stage. All zebrafish experiments were conducted in accordance with Stanford University's animal care guidelines and APLAC and IACUC approved animal protocol (no. 9935). The wild-type background Leopard was used throughout for transgenesis, mutagenesis and behavioural experiments as well as the crossing in of the *nacre* allele in cases in which transparency was required for imaging.

Molecular cloning, fish lines and transgenesis.

α-Tubulin panneuronal driver line.—Tg(α-tubulin:nls-Kal4FF) or Tg(α:nk) was produced through LR recombination with custom entry and destination vectors, as well as those provided by the tol2 kit 1.0 and 2.0[41]. In brief, the 2.6-kb fragment of the α-tubulin promoter was amplified by PCR from α-tubulin:gal4 plasmid (gift from S. Fraser[42]) and recombined with a modified less-toxic gal4 pME_Kal4FF (no. 781; tol2 kit v.2.0) with an additional nuclear localization sequence added by Gibson assembly to make pME_nls-Kal4FF. GFP was replaced by mCherry through PCR to create pDEST-cmlc-mCherry to reduce imaging artefacts of heart–GFP that occurred during the wide-field imaging of GCaMP.

Bicistronic transgenic GCaMP line (Tg(5×UAS:GCaMP6F-p2a-nls-mCherry)).—To improve registration, normalization of expression differences and tracking of individual densely packed neurons in moving samples, stable nuclear-localized mCherry was added 3′ of the ultrasensitive GCaMP6F[12] in frame between the unstable p2a motif to allow equal stoichiometric expression. This was placed under the control of a custom 5×UAS produced by replacing the UAS motifs p5E_10×UAS with 5×UAS from 5×UAS:GCaMP7a[43]. The localization of mCherry and dynamics of GCaMP6F in separate cellular compartments confirmed efficient separation through the bicistronic expression strategy.

zPSG line.—The zPSG line was created by crossing Tg(α-tubulin:gal4;cmlc2:GFP)[13] with Tg(5×ÚAS:GCaMP7a)[43] and Et(gSAIzGFFD109A), a gene trap line of the *igfn1* gene that expresses gal4 specifically in the trunk muscles, into the *nacre* background.

Panneuronal and panglial marker lines.—Tg(α-tubulin:gal4;cmlc2:GFP)[13] and Tg(GFAP:gal4;cmlc2:GFP)[13] were crossed to Tg(UAS:GFP) (a gift from H. Burgess) to give Tg(α-tubulin:gal4;UAS:GFP) and Tg(GFAP:gal4;UAS:GFP), respectively.

GFAP ablation line.—Tg(−7.3kb GFAP:epNTR-tagRFPT) was created to allow the specific ablation of GFAP-expressing cells. The 7.3-kb enhancer sequences 5′ to the start ATG of the GFAP acted as the promoter[44] to express the enhanced-potency nitroreductase (epNTR-tagRFPT[45]) (a gift from H. Burgess). These were recombined into a transgenesis vector expressing lens-promoter-driven mCherry as a transgenesis marker. The accurate localization of GFAP cells was confirmed by crossing the resulting transgenic line with Tg(GFAP:gal4;UAS:GFP).

MCH ablation line.—Tg(−5kb MCH:epNTR-tagRFPT) was created to allow the specific ablation of MCH2-containing neurons. The 5-kb enhancer sequences 5′ to the start ATG of the *Pmch2* gene[11] acted as the promoter to drive expression of epNTR. These were recombined into a transgenesis vector expressing lens-promoter-driven mCherry as a transgenesis marker. The accurate localization of MCH2 neurons was confirmed by immunostaining of fixed 8–9-dpf larva of the resulting transgenic line with a previously characterized MCH2 antibody[11] (Phoenix Pharmaceuticals, H-070–47, lot no. 01004).

Ependymal cells line.—Et(EP:mCherry) was identified through screening mCherry enhancer-trapped lines.

Transgenesis.—A mixture of tol2 plasmid with tol2 transposase RNA was injected into one-cell stage of wild-type or *nacre* zebrafish embryos as appropriate (FemtoJet microinjector, Eppendorf). Injected fish were screened after 48 h for their respective transgenesis marker and raised to adulthood (F_0). F_1 fish were selected by the appearance of strong expression or transgenesis markers in an outcross of F_0 fish, confirming germline transmission.

Mutants and CRISPR mutagenesis.—The *mchr1b*$^{-/-}$ mutant line from TILLING was obtained in the leopard background (ZIRC). CRISPR reagents were designed against MCHR1a and injected into MCHR1b-homozygous fish. Stable F_1 fish positive for mutations were identified through genotyping of fin clips before crossing into the zPSG line. Double-heterozygous fish were in-crossed for behavioural and imaging experiments and confirmations of genotype were performed post hoc after experiments by extraction of gDNA, PCR and then sequencing using primers straddling the mutation sites.

Behavioural assays.

Behavioural actimetry was performed as previously described, using Zebralab behavioural recording systems (Viewpoint Life Sciences)[46]. Larvae used in behavioural assays were housed in 1-l system water and fed with paramecia daily from 5 dpf onwards before experiments. Individual larvae were randomly chosen and placed in individual wells containing 2 ml of 1× E3 solution and acclimatized for at least 1 h in the recording system before assays. Larvae were recorded in ‘quantification’ mode with ‘detection sensitivity’ set

to 20, ‘burst’ 25, ‘freeze’ 3, ‘scale’ 20, ‘transparent’ checkbox checked and integration period set to 60 s. For 3-h drug assays, larvae were imaged with an infrared sensor for 1 h before addition of 20 µl of 100× drug, the effects of which were recorded for a further 2 h. For 24-h movies, randomly chosen control and test larva were placed in adjacent rows to minimize interdish microenvironment differences and fed with 100 µl of paramecia before starting the experiment at zeitgeber time 9 (ZT9) (ZT0, by convention, is the time of lights on). All larvae were fed with 100 µl of paramecia the next day at ZT3 to reduce variation caused by fasting conditions. The 09:00–23:00 light–dark cycle was controlled by day–night triggering with ‘sunrise’ and ‘sunset’ duration set to 60 s. At least two independent runs were performed for all behavioural assays, and visual inspection of all samples on completion of time points verified no assay condition resulted in fish with deteriorated health unless stated. The Excel (Microsoft) output was parsed into MatLab (Mathworks) for analysis with custom scripts (see Code availability).

Sleep deprivation.

Sleep deprivation was performed on 11–14-dpf zebrafish larvae by housing them in 15 ml of system water in a 15-ml conical centrifuge tube (Falcon; 352097) and removing enough liquid to create a bubble that spanned 2.5-ml gradations printed on the side of the tube. The conical tube was placed on a 360° platform rotating around the centre point at 0.5 Hz to move the bubble along the tube. Larvae were habituated to find the tip of the conical tube, to which the air bubble did not reach. When asleep, fish drift away from the tip towards the centre of the tube, where they are awoken by the air bubble turbulence and return to the less turbulent tip (see Extended Data Fig. 1b).

Wake maintenance.

Wake maintenance during circadian day or wake phase was performed to maintain good sleep consolidation during imaging on the subsequent night. To do this, fish arousal was maintained by a mechano-acoustical stimulus provided by a solenoid actuator (12 V, 1 A) striking the side of a Petri dish filled with 25 ml E3 solution (Extended Data Fig. 10a). This stimulus was randomized through a relay switch controlled by an Arduino UNO with a custom sketch (see Code availability) to prevent response adaptation and robust arousal per stimulus bout (randomization: 2–10 strikes, 500–950-ms interstrike interval and 30–45-s interval between strike bouts). The random stimulus was provided continuously from ZT2 until ZT13, before a 30-min rest before behavioural actimetry or mounting for selective plane illumination microscopy (SPIM) imaging.

Habituation.

Actimetry that was performed to test the effects of agarose mounting indicates that embedding leads to wake-stimulating effects, as manifested by sleep rebound after release from 1-d embedding (Extended Data Fig. 11b). This is consistent with our previous observations of wake fPSG traces in these restraint conditions in the absence of manipulations to promote sleep (data not shown). However, further testing showed that fish can habituate to agarose embedding and spontaneously fall asleep after 2–3 day–night embedding cycles. This habituation protocol is sufficient for untreated fish to express

specific sleep neural signatures, while under restraint within a 2-h recording window during the night.

Pharmacological reagents.

All reagents were prepared fresh on the day of the experiment and dissolved in E3 to create working solutions to be added to the experimental chamber, and compared to the addition of carrier-only controls. Gaboxadol (Sigma T101), MS222 (Sigma), mepyramine (Sigma P5514), promethazine (Sigma P4651), carbachol (Sigma C4382), eserine (Sigma E8375) and methoctramine (Sigma M105) were all dissolved in E3. H6408 (Bachem; H-6408.0001) was prepared with double-distilled (dd) H_20 (ddH_20) at 1 mM with a working concentration at 10 μM. Zolpidem (Sanofis Pharmaceuticals; active ingredient of the prevalent sleep drug Ambien) was a gift from S. Nishino, and stock solutions were prepared in DMSO. Effective concentrations and fish age (ranging from 7 dpf–14dpf) were chosen based on published data[47,48] or dose–response experiments driving behavioural sleep in the Viewpoint behavioural tracking system (Supplementary Table 1). At least two independent tests for all drug dose–responses were performed.

Injected MCH peptide (Phoenix Pharmaceuticals; 070–47, lot no. 429808) was prepared as a 1 mM working solution in ddH_20 supplemented with phenol red solution (Sigma; P0290) to confirm injection (see Extended Data Fig. 7h). Intracerebroventricular pulsatile injections (FemtoJet Microinjector, Eppendorf) were performed with zPSG larvae mounted in agarose.

Sample preparation and Ca^{2+} imaging.

All live imaging was captured with 7–14-dpf non-anaesthetized, non-paralyzed, agarose-restrained zebrafish larva using 1.5% LMP agarose (FMC BioProducts 50102) supplemented with 1% HEPES (Sigma H3375). If blood flow ceased or brain tissue became opaque during imaging (a classic sign of death), the zebrafish was excluded from further imaging or analysis. Corresponding behavioural experiments conducted before Ca^{2+} imaging have determined, in general, the good viability of zebrafish in response to the various pharmacological and sleep deprivation paradigms we used. Fish removed after two hours in agarose are healthy and viable, and can be grown to adulthood as required. Further checks were conducted with mounting and restraint in agarose for extended periods of up to 72 h; these larvae still showed fast escape responses from release (data not shown) and resume normal sleep–wake rhythms similar to sham-mounted (5 min in agarose and then released) siblings (Extended Data Fig. 11).

Telencephalon imaging.—Single-cell resolution imaging of the zebrafish larval telencephalon was performed on a Leica SP5 microscope using 488-nm and 594-nm laser lines. Fish were imaged dorsally at 2 Hz for 2 h in a single plane at the level of olfactory neuromasts (Fig. 1a, b), with the addition of drug or carrier 10 min into imaging. At least three independent experiments were performed per drug. *fPSG*. Wide-field light-sheet microscopy was performed on a custom-built light-sheet microscope based on the openSPIM design (www.openSPIM.org)[49], with modifications that enable temperature control and closed-loop perfusion (ThermoClamp-1, AutoM8 scientific). Head-restrained larvae were mounted within a 1-ml syringe creating a column of agarose that is extruded into

the path of the light sheet, and positioned for imaging with the dorsal side facing the camera. Unless stated, 12-mW 485-nm illumination was used and single planes were captured at 10× or 20× magnification for 2 h, at 1 or 2 Hz (as required). Preliminary analysis determined that single-plane imaging at the level of the habenula at 1 or 2 Hz was sufficient to identify the key events of PWS induction, whereas SBS and recordings that required the assessment of the visible telencephalon were taken at the level of the dorsal pallium 'olfactory' lateral-line clusters (Fig. 1a). For whole-brain imaging experiments, 6 planes were captured at 2.5-s intervals; the shortest interval that avoided substantial inertial jitter from moving the sample through the light sheet. Pharmacological reagents were added during imaging into the 10-ml volume of a chamber at 100×, and mixed through repeated aspiration with a Pasteur pipette without interruption of imaging. For full fPSG experiments, brain and spinal cord Ca^{2+} imaging acted as a proxy for EEG (fEEG), muscle-trunk Ca^{2+} imaging was the proxy for EMG (fEMG), fluorescence reflections from eye iridescence indicated saccades as a proxy for EOG (fEOG) and, as a proxy for ECG (fECG), a single *z*-plane was recorded through the green fluorescent heart at 10 Hz for 5 min before and after the main fPSG imaging period, to capture the heart rate.

Cell ablation.

Seven-dpf Tg(MCH:epNTR-tagRFPT) larvae that were positive for red fluorescent lenses, and sibling red-lens-negative larvae acting as controls, were treated at 26.5 °C for 24 h with 10 mM metronidazole (MP Biomedical 02155710) in E3 supplemented with 1% DMSO at a maximum density of 12 larva in 10 ml. Treated larvae were briefly washed in 1× E3 solution before transferred to 10 ml of 1× E3 solution overnight for recovery, before behavioural or imaging experiments. In initial experiments, red cells were confirmed before ablation (as was the absence of cells after ablation in the same fish) by live imaging on an SP5 confocal microscope (Extended Data Fig. 8b, c). The attempts to ablate ependymal cells with Tg(GFAP:epNTR-tagRFPT) were performed in a similar fashion.

Analysis.

Viewpoint.—Visual calibration was performed for each Viewpoint system such that each active swim movement of a larva resulted in a timecount in the recorded parameter 'Middur'. This resulted in the detection sensitivity of '20' used throughout. Sixty-second bins of activity were summed for 10 min to give averages of seconds of activity per 10 min. Sleep was defined as more than 1 min of continuous inactivity, which has previously been established as a reliable definition[5,7,9]. Thus, sleep was defined as no movement detected in Middur in a given 60-s bin, and summed into 10-min periods to show the average number of minutes per 10 min across day and night. Total activity (in seconds of activity per minute) and sleep were summed as a function of day and night, and displayed as box plots. These reports are generated in an automated fashion from the raw output from Viewpoint by running custom MatLab scripts (see Code availability).

Bicistronic GCaMP analysis.—Analyses were performed in MatLab (Mathworks) on image sequences converted from Leica format to .tiff format using Fiji (ImageJ). Frames were motion-corrected using either the moco plugin in Fiji or inverse fast Fourier transform in MatLab. To quantify synchronicity and SBS dynamics, we developed two indices: the

coherence index and the ITI, respectively. For the coherence index, we reasoned that increased synchronicity relates to an increased proportion of neurons being active during a given epoch, when a given epoch contains at least one active neuron. Using the stable red channel, individual dorsal pallium nuclei were either automatically selected by standard adaptive thresholding segmentation or manually traced, depending on performance of the segmentation. Two-pixel-wide GCaMP masks were created by morphogenesis of nuclei masks through structural element dilation, and removing the original nuclei mask. These masks were applied to the GCaMP channel to capture average pixel intensity (F_t). Changes from baseline fluorescence intensities ($F_t - F_0$) were normalized by their minimum value (F_{min}) extracted in each individual trace as a $\Delta F/F$ proxy for neural activity. Ca^{2+} dynamics were detrended and thresholded at 1.5 s.d. above baseline fluorescence (10th percentile) to define a discrete 'spike'. The number of active neurons was summed in each epoch, and the coherence index was quantified as the percentage of spikes that appear in epochs in which more than 50% of neurons are simultaneously activated. For ITI, region of interests (ROIs) containing either individual neurons (SP5) or the two dorsal pallium hemispheres (SPIM) were manually traced using an s.d. projection. Ca^{2+} dynamics were detrended and thresholded at one s.d. above baseline fluorescence (10th percentile) to define a discrete spike. We then measured, for the entire duration of the movie, the duration between these bursts of activity in each ROI and averaged across all ROIs to calculate the average ITI at manually defined periods, representing baseline or treatment. A larger ITI indicates extended periods of inactivity and a slowing of the overall frequency of bursts (see Supplementary Fig. 1 for schematics). Independent component analysis and PCA by singular value decomposition were performed using built-in MatLab functions.

fPSG.—As we sacrifice spatial resolution for increased coverage at 10× magnification, we decided to manually trace masks covering broad areas of the brain in a single slice of a maximum projection for volumetric recordings. Masks were applied to the GCaMP channel and $\Delta F/F$ measurements were determined as above for nuclei-derived masks. Trunk-muscle masks were also drawn separately to trace muscle tone, and eye movements were manually scored from video replay. For analysis of heart rate, the mask of one heart ventricle was traced (Extended Data Fig. 4g). This was used to quantify the changing fluorescence as the heart moved within the mask. The peak analysis algorithm of MatLab was used to extract the timing of peaks to derive heartbeat rate and interbeat intervals (Extended Data Fig. 4h). The coefficient of variation was calculated as an indication of the variability of the heartbeat.

PMT dynamic assays.—Two clear independent neural activity markers were used to determine the effect of pharmacological MCHR block, MCH2-neuron ablation and MCHR knockout on the ability of the brain to transition to PWS sleep. The first of these was the midline ependymal cell activation and the second was the induction of the brain-wide PMT wave. We determine the time of onset of these features specifically to when the ependymal cell surge reached the midbrain–hindbrain boundary, and when the PMT wave reached the tectum neuropil. In cases in which neither event occurred in the 2-h period following drug treatment (which was almost never the case under control conditions), the value of two hours was recorded as the activation time—thus, in effect representing an under-quantification of the true delay to the induction of these brain signatures by the MCH treatments.

Statistics.

Statistics were performed on raw data in MatLab using functions from the Statistical Toolbox. Explicit tests were not performed to predetermine sample size. Neither randomization of samples nor blinding was done for the automated analysis. For comparison of two conditions, the Student's *t*-test, paired *t*-test or non-parametric Wilcoxon rank-sum test was performed, as appropriate. For comparison of group means, one-way analysis of variance (ANOVA) with Tukey's post hoc comparison or repeated measures ANOVA was performed, as appropriate. To compare discrete proportion outcomes between groups, the χ^2 test was used. Significance was determined with the 0.05 alpha level for all statistical tests.

Reporting summary.

Further information on research design is available in the Nature Research Reporting Summary linked to this paper.

Data availability

Data that support the findings of this study are available as Supplementary Information and Source Data. The supplementary videos are linked in the Supplementary Information and are available for downloading at https://drive.google.com/open?id=1CQGSFzxm39KCvN9D_XwJR2rOY6hS7oC5. Any other relevant data are available from the corresponding author upon reasonable request.

Code availability

Code for custom Viewpoint protocols, Arduino sketches, FIJI macros and MatLab programs are available from https://github.com/louiscleung.

Extended Data

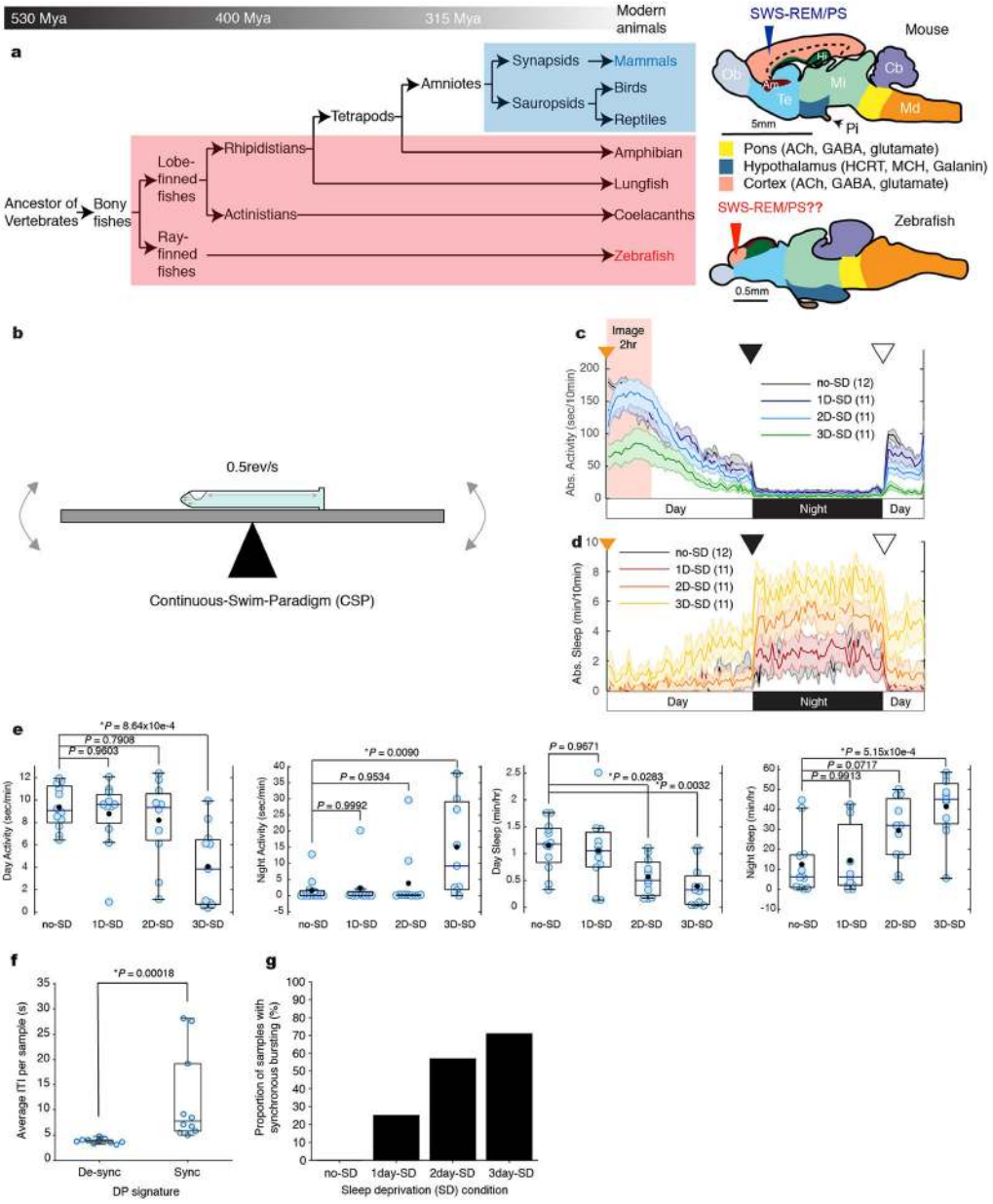

Extended Data Fig. 1 |. Sleep deprivation by the continuous-swim paradigm.

a, Left, evolutionary tree depicting current description of SWS and PS/REM sleep in amniotes. Right, schematic showing lateral view of major brain regions and neurochemistry that is implicated in sleep. Ob, olfactory bulbs; Am, amygdala; Hi, hippocampus; Te, telencephalon; Mi, midbrain; Cb, cerebellum; Md, medulla. **b**, Schematic showing the sleep deprivation (SD) setup (see Methods). **c**, **d**, Behavioural actimetry verifies that the sleep rebound induced by sleep deprivation causes decreasing wake and increasing sleep amounts as a function of number of days of sleep deprivation. Trial-averaged traces across 24 h after zebrafish were released following 1 day ($n = 11$, purple (**c**) or red (**d**)), 2 days ($n = 11$, blue (**c**) or orange (**d**)) or 3 days ($n = 11$, green (**c**) or yellow (**d**)) of sleep deprivation, against non-sleep-deprived sibling controls ($n = 12$, black). Mean activity is expressed as seconds of

activity per 10-min bin (bold line) ± s.e.m. (shaded), per condition. Mean sleep amount is expressed as minutes of sleep per 10-min bin (bold) ± s.e.m. (shaded), per condition. The black triangle depicts the day-to-night transition, the white triangle depicts the night-to-day transition and the orange triangle shows the time of feeding. Red box in **c** indicates the equivalent time at which Ca^{2+} imaging was conducted. **e**, Box plots showing the spread of total amounts of activity and sleep between non-sleep-deprived and sleep-deprived conditions, separated out by day and night. Blue lines denote median and black circles present the mean value for the group. $*P < 0.05$, one-way ANOVA with 0.05 alpha level and Tukey's post hoc multi-comparison testing. **f**, Scatter plot of average ITI from desynchronized and synchronized brain activities. $*P < 0.05$, two-sided Wilcoxon rank-sum test, $n = 10$ fish per condition. **g**, Bar chart showing proportion of samples that displayed SBS within 2 h of release from non-sleep-deprived, 1-day, 2-day and 3-day sleep deprived conditions.

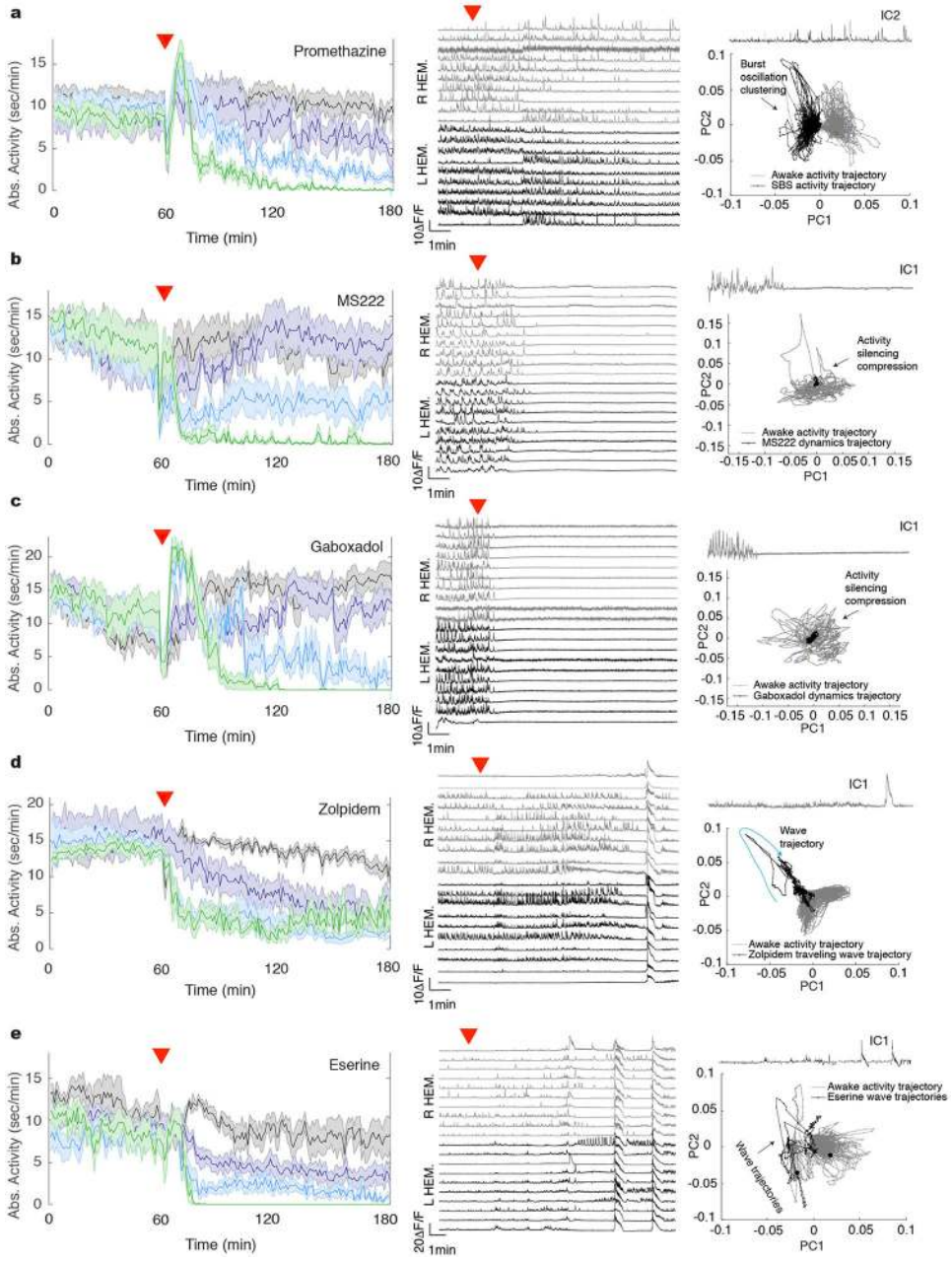

Extended Data Fig. 2 |. Hypnotics produce distinct neural dynamics, including synchronous activity, travelling waves and broad silencing.

a–**e**, Left, representative activity from 3-h recordings in which drugs were added after 1 h (red triangle) to freely swimming zebrafish. Activity traces are expressed as the number of seconds of activity per 10-min time bin, and plotted as mean (solid line) ± s.e.m. (shaded) per dose of promethazine (**a**, $n = 24$ fish), MS222 (**b**, $n = 24$ fish), gaboxadol (**c**, $n = 24$ fish), zolpidem (**d**, $n = 24$ fish) and eserine (**e**, $n = 24$ fish) from low to high doses (black < purple < blue < green; see Supplementary Table 1 for concentrations), showing the induction of dose-responsive behavioural sleep. Middle, representative time-aligned $\Delta F/F$ traces of20 randomly selected dorsal pallium neurons (red triangle indicates the addition of drug after 10

min). Promethazine induced mild synchronization of dorsal pallium neurons, MS222 and gaboxadol induce total silencing, and zolpidem and eserine induced travelling waves. Right, neural signature across all time points represented by the first independent component (top) or replotted on two-dimensional phase space following PCA (bottom, grey lines and black lines depict wake versus sleep trajectories, respectively). See Supplementary Information for reproducibility information.

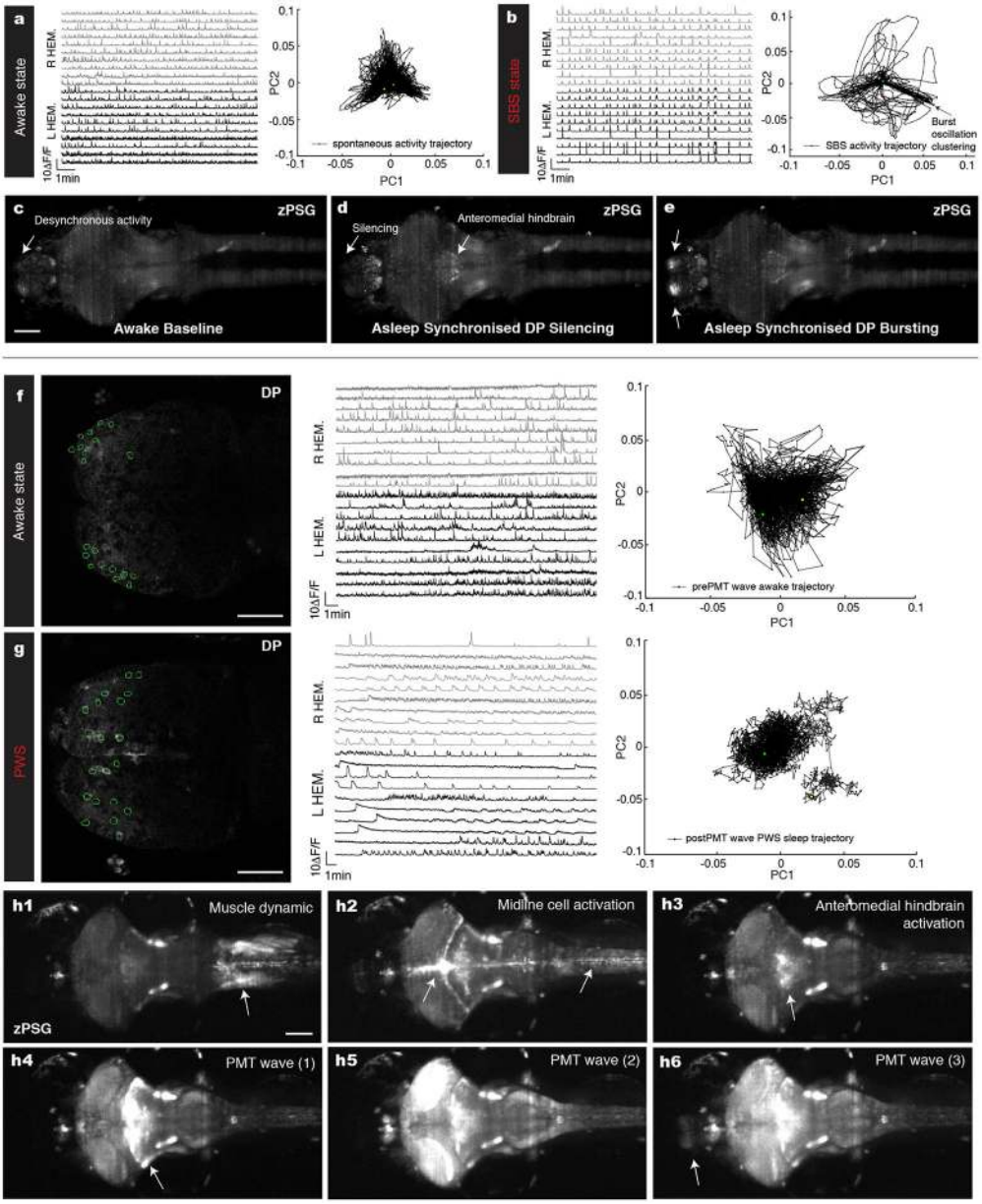

Extended Data Fig. 3 |. fPSG of SBS and PWS.

a, **b**, Dorsal pallium signature of wake (**a**) versus SBS (**b**) with time-aligned $\Delta F/F$ traces of 20 randomly selected masks. Neural signature plotted in two-dimensional phase space following PCA. **c**–**e**, Typical light-sheet images of a single *z*-slice through brain and trunk muscle during wake (**c**) and during SBS (**d**, **e**). Scale bar, 100 μm. **f**, **g**, Dorsal pallium signature of wake (**f**) versus PWS (**g**) with time-aligned $\Delta F/F$ traces of the 20 masks depicted in the left image. Pre- versus post-PMT-wave synchronicity indices: ITI, 2.88 ± 2.14 s versus 2.96 ± 1.35 s, $P = 0.792$, Wilcoxon rank-sum test, $n = 5$ fish; coherence index, 1.32% ($n = 1{,}024$ spikes) versus 1.08% ($n = 1{,}065$ spikes); $P > 0.05$, χ^2 test. Neural signature plotted in two-dimensional phase space following PCA. Scale bars, 50 μm. **h**, Subpanels h1–h6 show selected frames from a typical fPSG volume acquisition of PWS in

which *z*-planes have been compressed into a maximum projection. Frames depict preceding events up until, and through, the PMT-wave transition to sleep. Arrow in h1 indicates muscle rostrocaudal wave; arrows in h2 indicates coordinated ependymal cell activation; arrow in h3 indicates anterior hindbrain activation; arrow in h4 indicates wave initiation; arrow in h6 indicates propagation to the dorsal pallium (see Supplementary Information for detailed description). Scale bar, 100 μm. See Supplementary Information for reproducibility information.

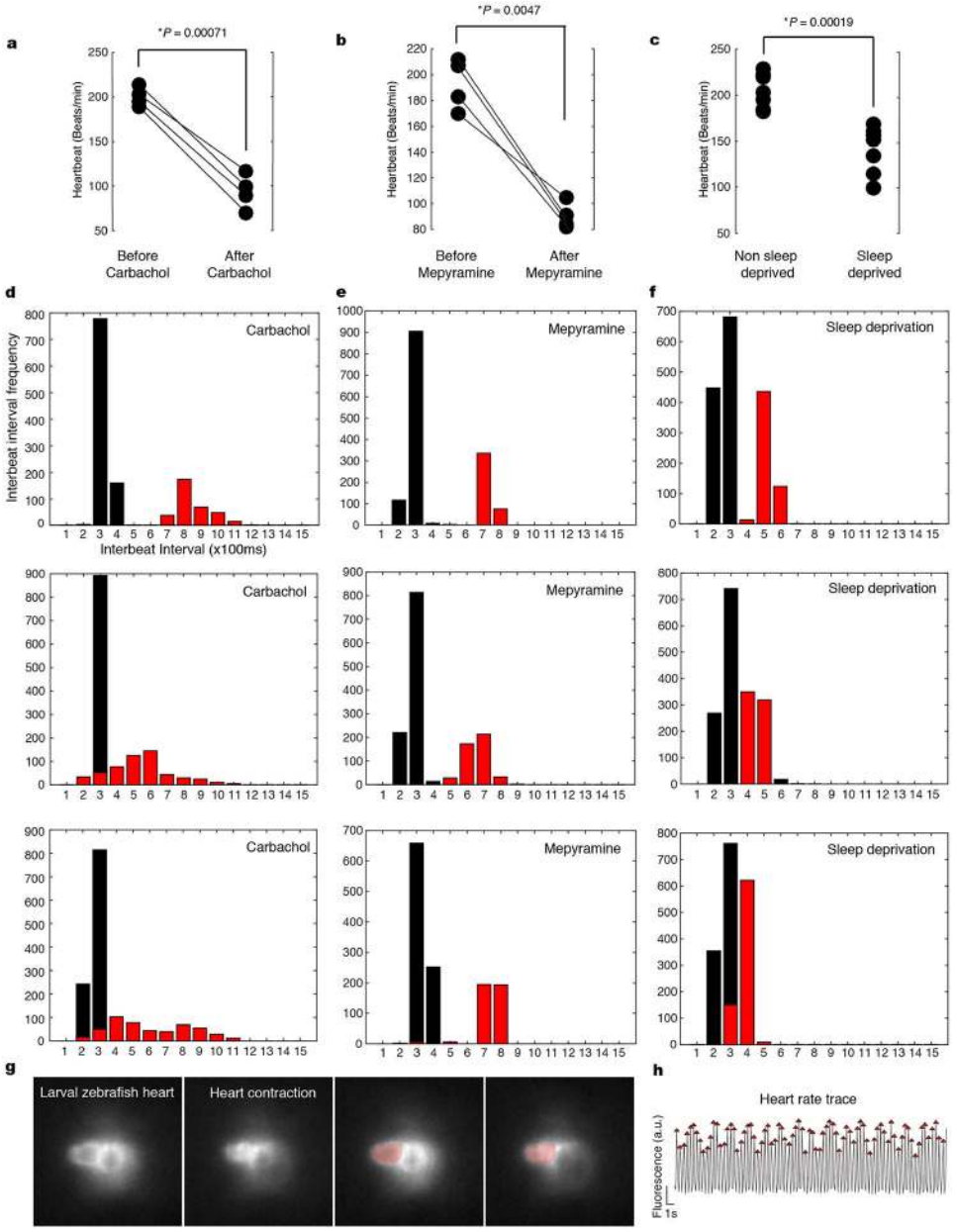

Extended Data Fig. 4 |. Heart rate analysis.

a–**c**, Heart rate analysis before and after carbachol treatment (**a**) (*$P < 0.05$, two-sided paired *t*-test, $n = 4$ fish), mepyramine treatment (**b**) (*$P < 0.05$; two-sided paired *t*-test, $n = 4$ fish) and with or without sleep deprivation (**c**) (*$P < 0.05$; two-sided Student's *t*-test, $n = 7$ non-sleep-deprived and 7 sleep-deprived fish). **d**–**f**, Histograms comparing the distribution of interbeat interval before (black bars) and after (red bars) treatment with carbachol (**d**)or mepyramine (**e**), and with (red bars) or without (black bars) sleep deprivation (**f**). Three representative histograms are shown for each condition. **g**, Representative images from heart rate capture showing ventricular contraction and the drawing of a mask (red) to measure fluorescence changes from the green fluorescent heartbeat. **h**, An illustrative plot of

fluorescence variation measured by the mask, overlaid with the result of running peak analysis (red triangles) from which the heart rate and interbeat interval are derived.

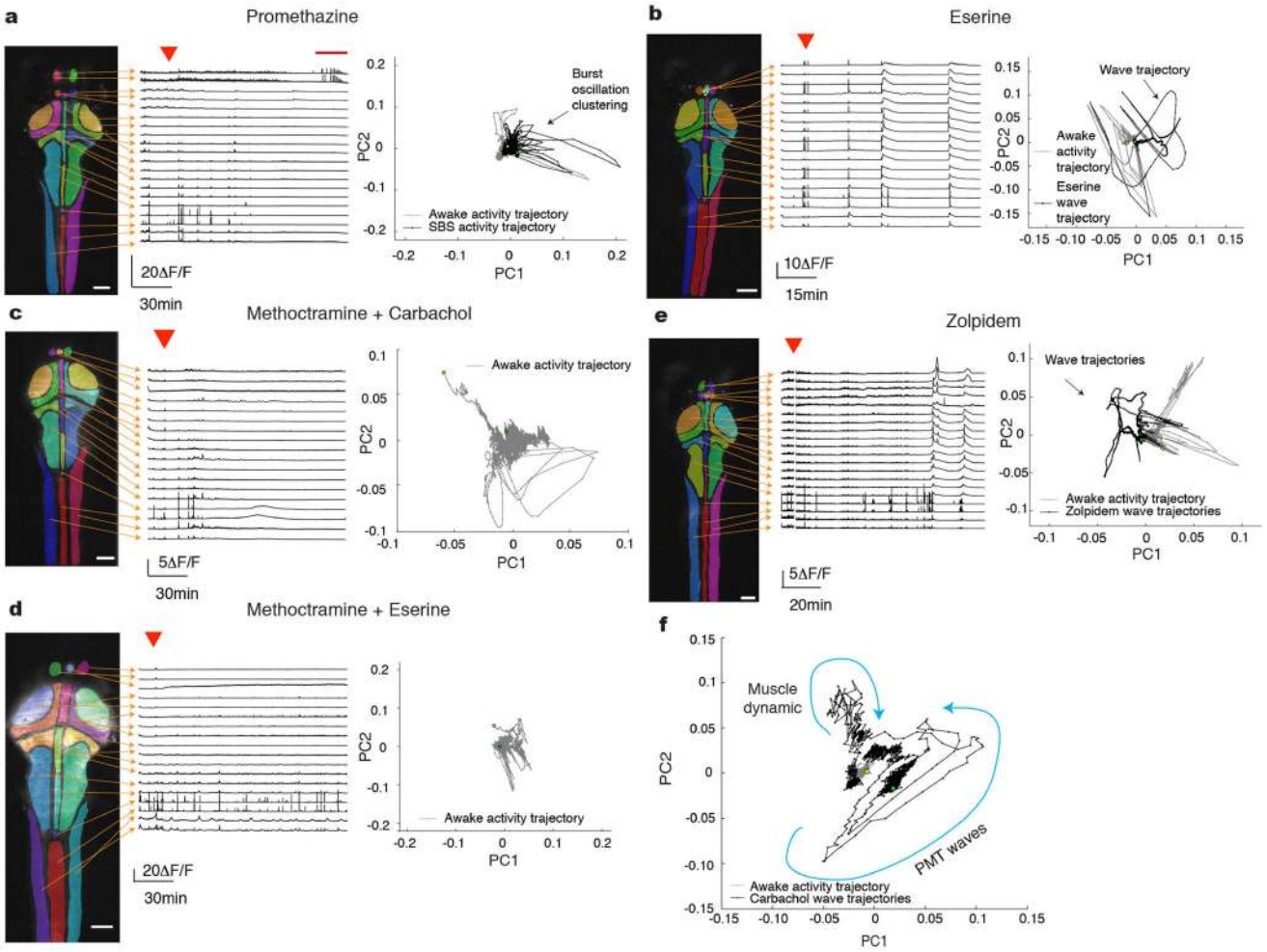

Extended Data Fig. 5 |. Brain-wide imaging with additional hypnotics.

a, Brain-wide single-plane imaging of promethazine-stimulated zebrafish. Promethazine induces bilaterally synchronous burst dynamics in the dorsal pallium (red bar). Left, masks used to extract Ca^{2+} transient traces shown in the middle panel. Dynamics are summarized by PCA (right). **b**, Brain-wide single-plane imaging of eserine-stimulated zebrafish. Eserine induces PMT waves. Left, masks used to extract Ca^{2+} transient traces shown in the middle panel. Dynamics are summarized by PCA (right). **c**, Brain-wide single-plane imaging of carbachol-stimulated zebrafish pre-incubated with methoctramine. Methoctramine prevents carbachol-induction of the PMT wave. Left, masks used to extract Ca^{2+} transient traces shown in the middle panel. Dynamics are summarized by PCA (right). **d**, Brain-wide single-plane imaging of eserine-stimulated zebrafish pre-incubated with methoctramine. Methoctramine prevents the eserine-induced PMT dynamics. Left, masks used to extract Ca^{2+} transient traces shown in the middle panel. Dynamics are summarized by PCA (right). **e**, Brain-wide single-plane imaging of zolpidem-stimulated zebrafish. Zolpidem induced multiple PMT waves. Left, masks used to extract Ca^{2+} transient traces shown in the middle panel. Dynamics are summarized by PCA (right). Red triangles show the point at which the drug was added. **f**, PCA by singular value decomposition of the fPSG PMT signature seen in Fig. 3e. Distinct steady states for wake (grey lines) and PWS sleep (black lines) can be

separated, as can marked trajectories of muscle and brain travelling waves (blue lines). See Supplementary Information for reproducibility information. Scale bars, 100 μm.

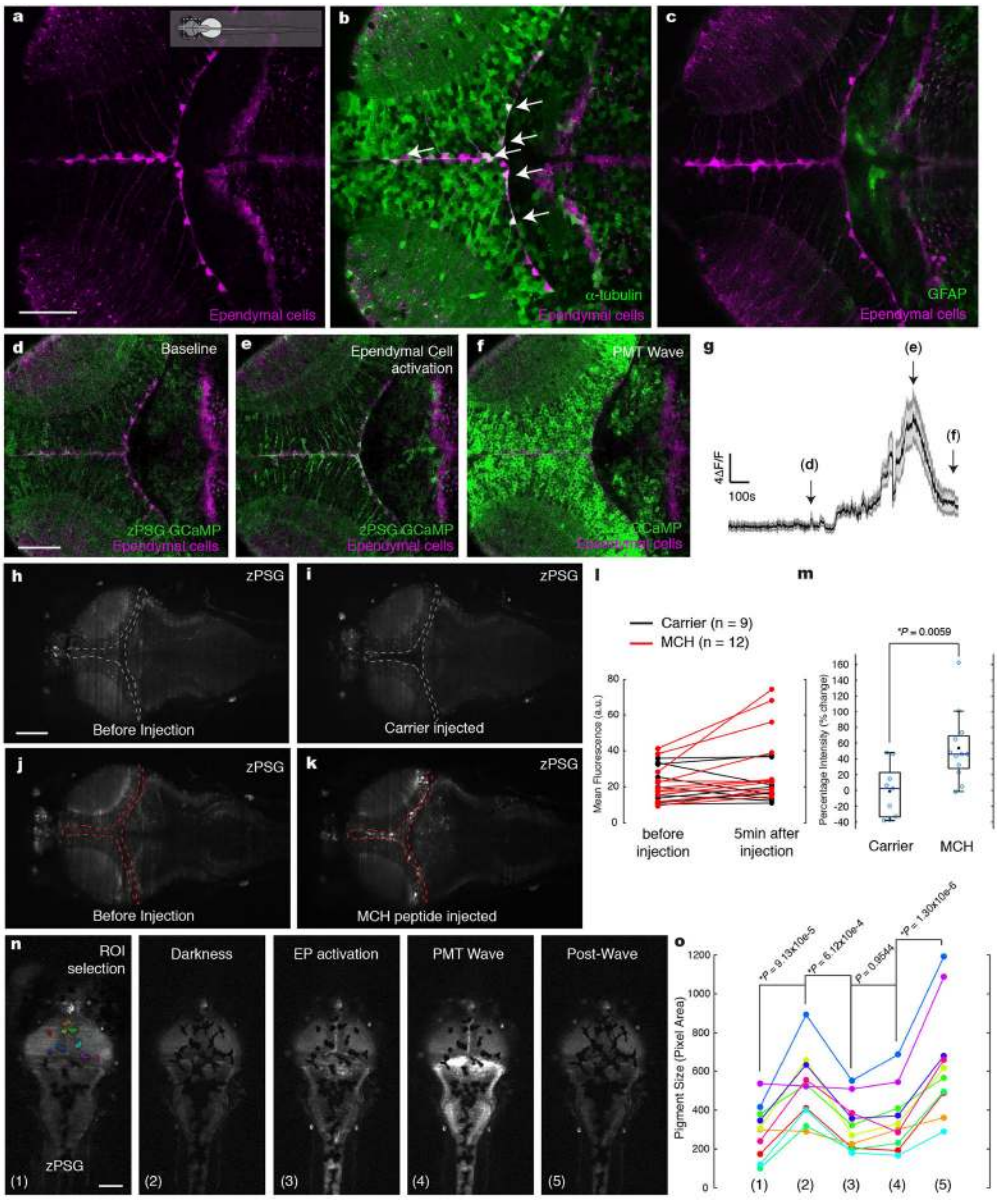

Extended Data Fig. 6 |. Ependymal cell activation is tightly correlated to the PMT wave and can be induced by the neuropeptide melanin concentrating hormone.

a, Dorsal view of a single slice through the optic tectum of Et(EP:mCherry) fish. Inset dashed box indicates location along the anteroposterior axis. Scale bar, 50 μm. **b**, Slice through the optic tectum of a 7-dpf Et(EP:mCherry);Tg(α-tubulin:gal4;UAS:GFP) triple transgenic fish. Arrows, mature ependymal cells (magenta) co-expressing α-tubulin (green). **c**, Slice through the optic tectum of a 7-dpf Et(EP:mCherry);Tg(GFAP:gal4;UAS:GFP) triple transgenic fish. Mature ependymal cells largely do not overlap with GFAP-positive cells. **d**–**g**, Ventricular cells activated before the PMT wave are EP:mCherry-positive ependymal cells. Confocal *z*-slice through a 7-dpf zPSG;EP:mCherry double transgenic fish before stimulation (**d**), ependymal cell activation (**e**) and PMT wave (**f**). **g**, Mean ± s.e.m. $\Delta F/F$ trace of five randomly selected double-positive cells showing the transient activation of

ependymal cells before the PMT wave. Arrows indicate the time from which images shown in **d**–**f** are taken. Scale bar, 50 μm. **h**–**m**, MCH peptide induces activation of ependymal cells. Representative maximum projection through SPIM volume acquisition before (**h**, **j**) and 5 min after intracerebroventricular injection with carrier (**i**) or MCH peptide (**k**). **l**, Mean normalized fluorescence between carrier ($n = 9$ fish) and MCH ($n = 12$ fish) groups from the peritectoventricular zone (dashed lines) before and after injection. **m**, Box plot of normalized fluorescence percentage change values between carrier- and MCH-injected groups with black circle depicting mean. $^*P < 0.05$; two-sided Student's *t*-test. Scale bar, 100 μm. **n**, Pigment contraction is tightly coupled to discrete activations during PMT-wave dynamics. Representative frames selected from a single *z*-recording of a pigmented zebrafish during a PMT wave; (1) colour-coded selection of all pigments covering the optic tectum as a representative sample; (2) during darkness and baseline activity, pigments are spread out and cover more pixel area; (3, 4) pigments contract with ependymal cell activation and the PMT wave; (5) when the wave abates, pigments re-spread. Scale bar, 100 μm. **o**, Quantification of pixel area plotted with representative colour from subpanel (1) in **n** at the different time points shown in subpanels (1) to (5) in **n**. $^*P < 0.05$, repeated-measures ANOVA, $n = 10$ pigments. See Supplementary Information for pigment dynamics description and reproducibility information.

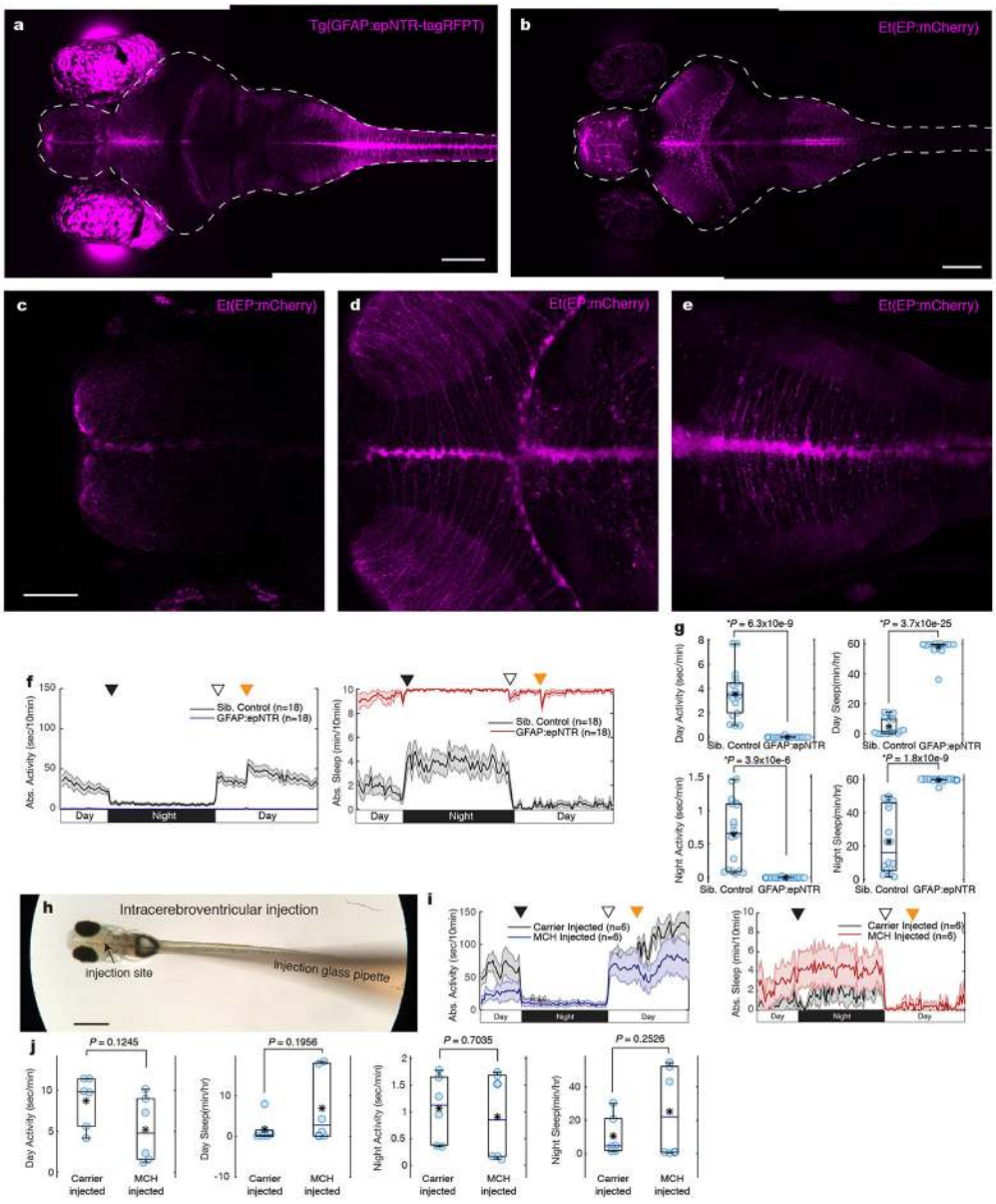

Extended Data Fig. 7 |. Characterization of GFAP:epNTR and EP-mCherry transgenic fish.
a, Dorsal view of maximum projection of a 7-dpf Tg(GFAP:epNTR-tagRFPT) zebrafish used to ablate GFAP-positive cells. Scale bar, 100 μm. **b**, Maximum projection of a 7-dpf Et(EP:mCherry) zebrafish expressing mCherry in putative ependymal cells. Scale bar, 50 μm. **c**, Single *z*-slice of dorsal pallium of Et(EP:mCherry) fish. mCherry cells located on the ventricular surface of the telencephalic neuroepithelium and present in the midline. Scale bar, 50 μm. **d**, Single *z*-slice of optic tectum parenchyma of Et(EP:mCherry) fish. mCherry cells are located all along the ventricular surface comprising the ependyma. Long thin processes invade the mesencephalic parenchyma, which suggests the morphology of non-neuronal glial cells and (in particular) the specialized ependymal cell type, tanycytes. **e**, Single *z*-slice of hindbrain of Et(EP:mCherry) fish. mCherry cells are located all along the midline ventricular surface, representing the ependyma stretching to spinal cord central

canal. Long thin processes suggest the morphology of non-neuronal cells. **f**, **g**, Actimetry shows GFAP-cell-ablated fish are irreversibly immobile without recovering activity during daytime. Mean activity is expressed as seconds of activity per 10-min bin (bold) ± s.e.m. (shaded), per condition. Mean sleep amount is expressed as minutes of sleep per 10-min bin (bold) ± s.e.m. (shaded), per condition. The black triangle depicts the day-to-night transition, the white triangle depicts the night-to-day transition and the orange triangle shows the time of feeding. Box plots showing total activity and sleep for sibling controls versus GFAP-cell-ablated larva. Blue line denotes median and black circles indicate the mean value (**g**). $*P < 0.05$, two-sided Student's *t*-test, $n = 18$ sibling control and 18 GFAP:epNTR fish from two independent experiments. **h**, Photograph at 4× magnification of a restrained 7-dpf zebrafish receiving an intracerebroventricular injection of MCH solution with phenol red solution (pale red colour in the photograph). The ventricle is slightly expanded as a result of injection. Scale bar, 500 μm. **i**, **j**, Behavioural actimetry shows MCH-injected larvae are less mobile and sleep more during the first day and night after injection, but mostly recover by the second day. Box plots showing total activity and sleep for carrier- versus MCH-injected larva. Blue line denotes median and black asterisks indicate the mean value (**j**). $P > 0.05$, two-sided Student's *t*-test, $n = 6$ carrier- and 6 MCH-injected fish.

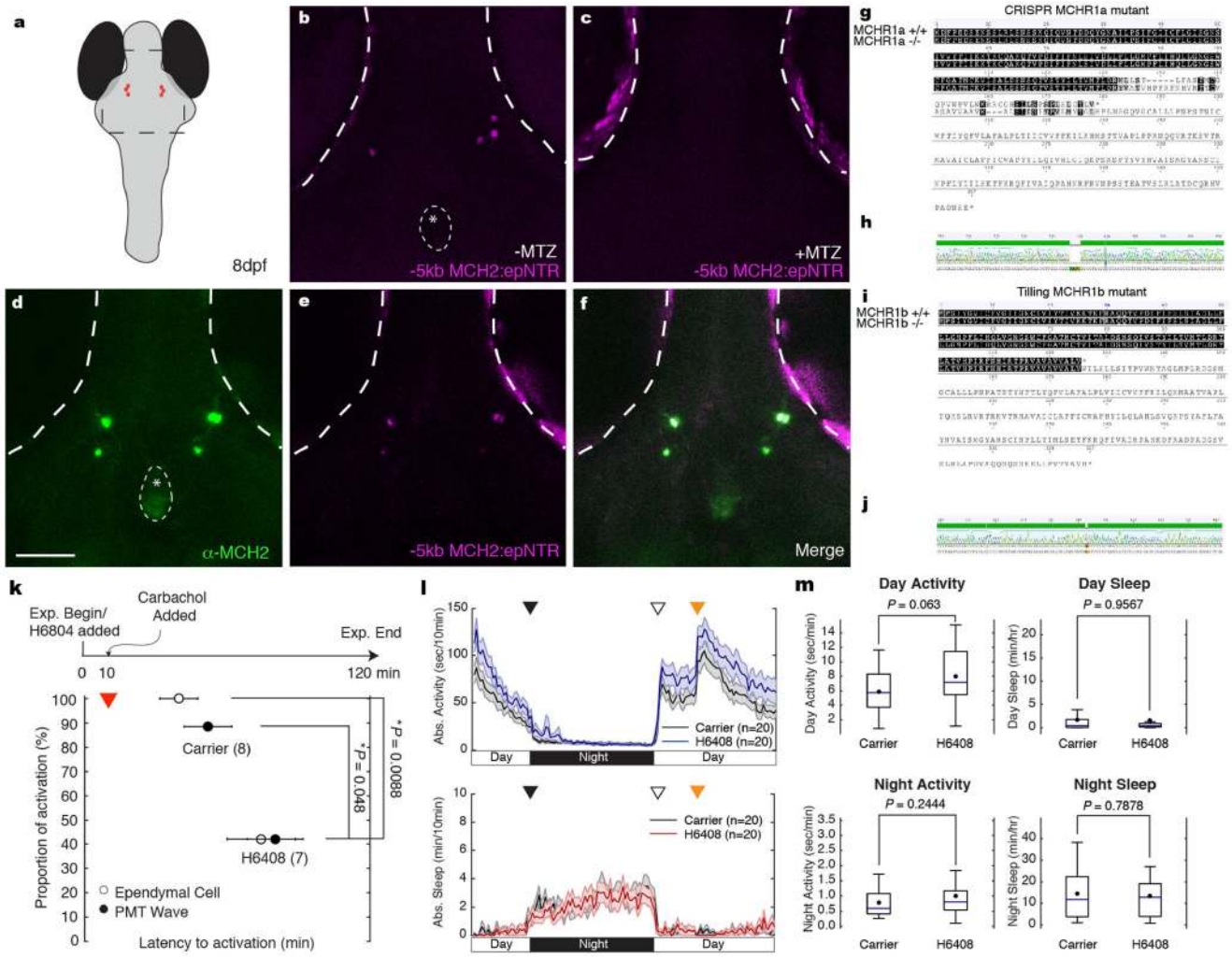

Extended Data Fig. 8 |. Characterization of MCH:epNTR, H6408 and *mchr1a mchr1b* double mutants.

a, Schematic of the location of MCH-positive cells in the lateral hypothalamus of the zebrafish larvae. **b**, Confocal maximum projection shows MCH cells from the Tg(−5kbMCH:epNTR-tagRFPT) transgenic fish before treatment with the ablation agent metronidazole (MTZ). Faint signal of projections to the pituitary are seen (dashed region and asterisk). Scale bar, 50 μm. **c**, MCH cells are ablated in Tg(−5kbMCH:epNTR-tagRFPT) larva treated with metronidazole. **d**–**f**, Tg(−5kbMCH:epNTR-tagRFPT) larva stained with MCH antibody show lateral hypothalamic location and projection to the pituitary gland (**d**) (green) co-localizing to tagRFP-T expression(**e**, magenta; **f**, white). **g**, Alignment of wild-type MCHR1a protein sequence and predicted truncated mutant protein resulting from CRISPR deletion. **h**, Sequencing confirmation of loss of TATG sequence from exon 2 of *mchr1a* gene from genotyping of homozygous MCHR1a mutant. **i**, Alignment of wild-type MCHR1b protein sequence and predicted truncated mutant protein resulting from TILLING mutant with early stop codon. **j**, Sequencing confirmation of TGG to TGA substitution from exon 1 of *mchr1b* gene from genotyping of homozygous MCHR1b mutant. **k**–**m**, MCHR-antagonist (H6408)-treated fish display increased activity and disrupted onset of ependymal

cell and PMT-wave dynamics. **k**, Top, timeline of experiment and addition of pharmacological agents during the 2-h Ca^{2+} imaging experiment (red triangle indicates the addition of carbachol). Bottom, proportion of activation of ependymal cells (open circle) and/or PMT wave (filled circle), witnessed in the imaging session between carrier control (n = 8 fish) and H6408 (n = 7 fish) is plotted against the mean latency to activation (in min) ± s.e.m. *P < 0.05 χ^2 test. **l**, Top, actimetry of wild-type zebrafish (n = 20) treated with carrier versus MCHR antagonist (H6408; n = 20) in 10-min bins over a 24-h period, showing mean seconds of activity per bin (bold) ± s.e.m. (shaded). Bottom, sleep depicted as minutes of sleep per 10-min bin (bold) ± s.e.m. across a 24-h period. Black triangle depicts the day-to-night transition, white triangle depicts the night-to-day transition and the orange triangle shows the time of feeding. **m**, Box plots showing spread of total activities and sleep between between carrier (E3)-stimulated versus H6408-treated groups, separated further by day and night. Blue lines denote median and black circles indicate the mean value. *P < 0.05, two-sided Student's t-test. See Supplementary Information for reproducibility information.

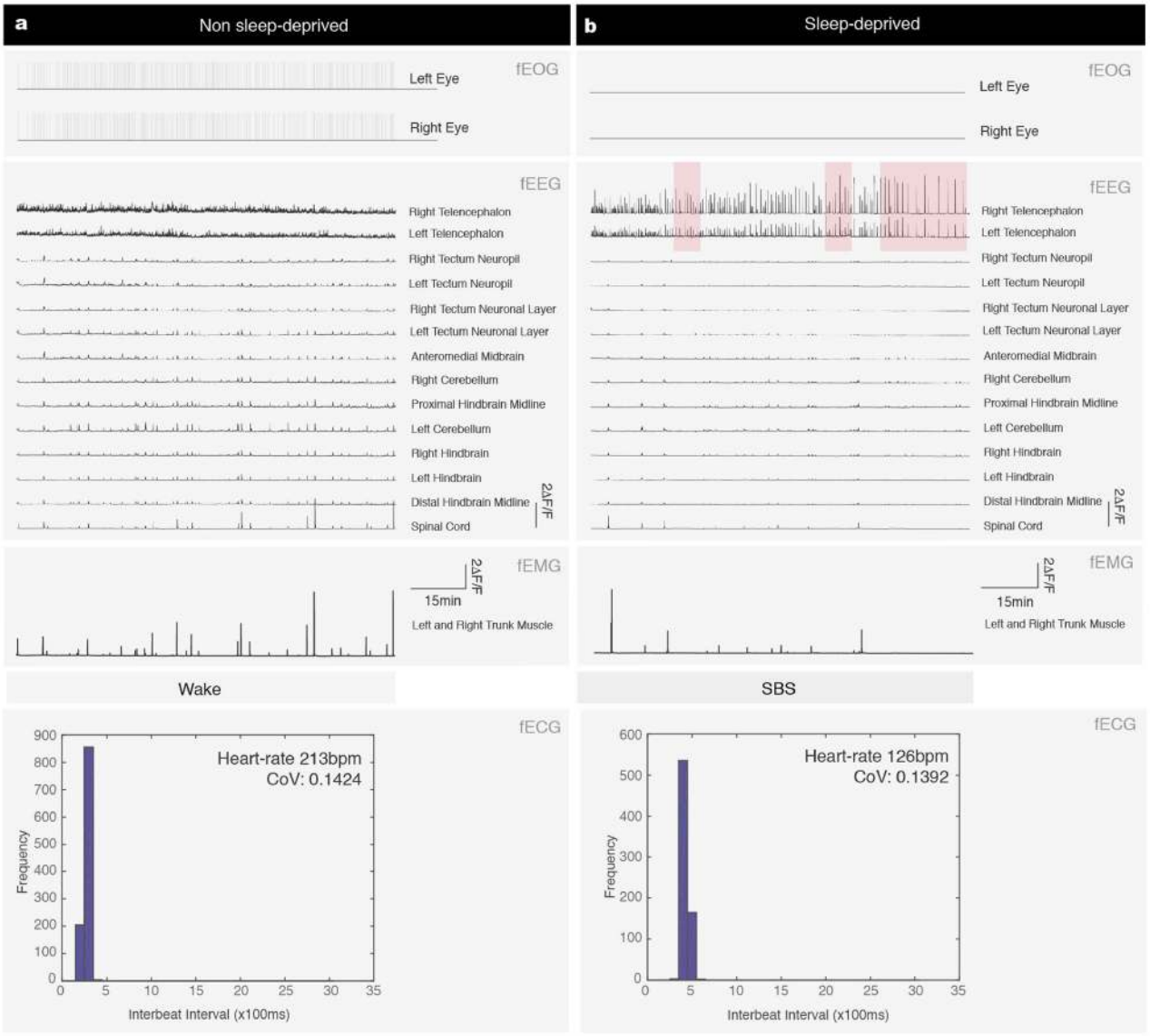

Extended Data Fig. 9 |. fPSG comparison of induced SBS in non-sleep-deprived and sleep-deprived fish.

a, **b**, Representative fPSG recording of non-sleep deprived (**a**) and sleep-deprived zebrafish (**b**) during normal night phase. Activity traces from fEOG (top), fEEG (middle) and fEMG (middle). fEEG and fEMG are $\Delta F/F$ traces from 14 masks covering broad brain regions (as labelled), with integration of neuronal activity across 1-s bins. Heart rate was measured immediately before imaging, and interbeat interval distribution is shown with coefficient of variation (CoV) (bottom). Transient synchronous bursting was detected (red boxes for example) between infrequent muscle twitches and broad brain arousal events. See Supplementary Information for reproducibility information.

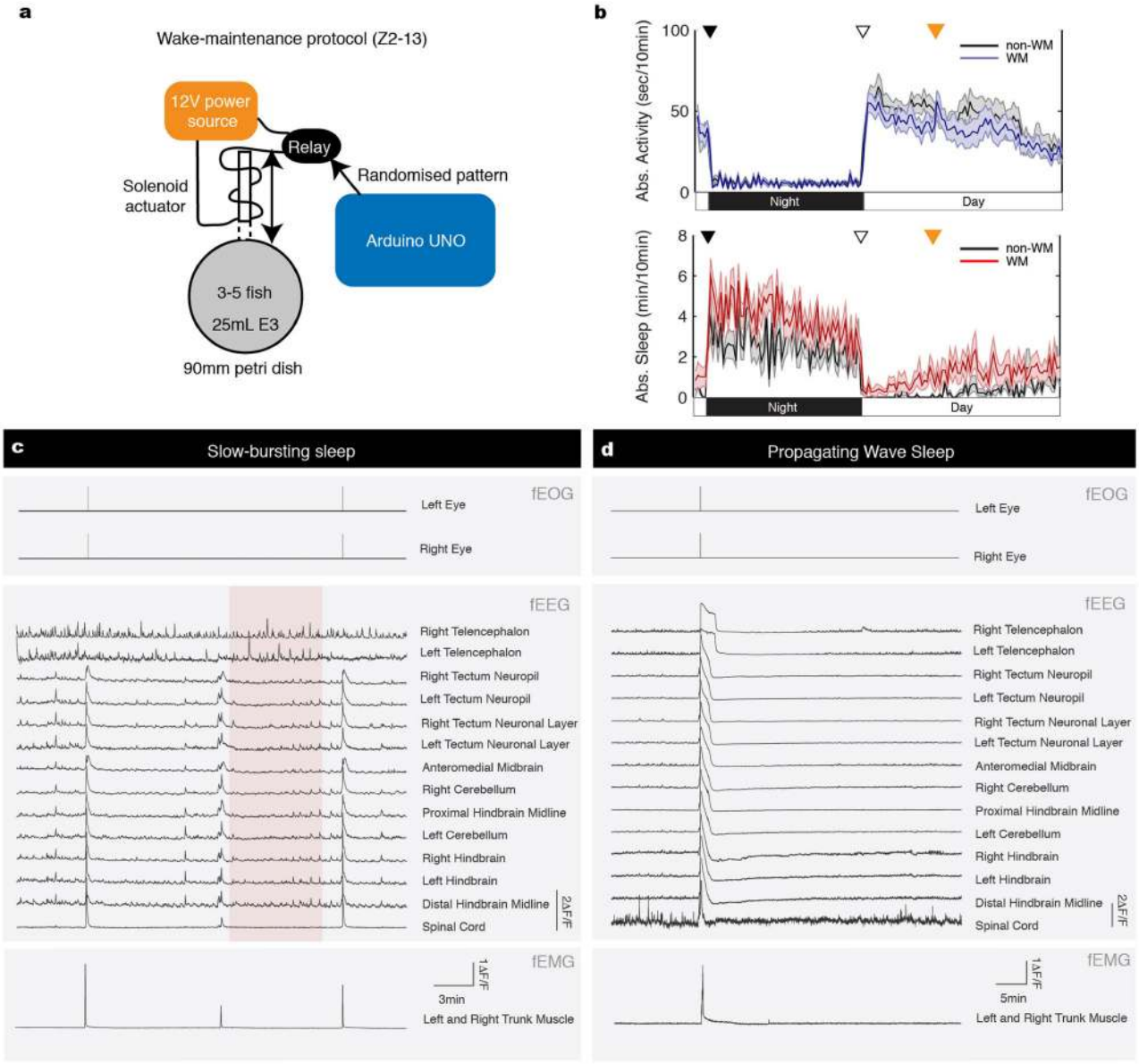

Extended Data Fig. 10 |. SPIM of wake-maintained larvae reveal SBS and PWS signatures during normal night.

a, Schematic of wake-maintenance apparatus adopting randomized mechano-acoustical stimulus during the day phase to consolidate wake, and thus sleep in the night phase for imaging. **b**, Representative actimetry of wild-type zebrafish not treated with the stimulus (n = 12 fish) with actimetry of wild-type fish treated with the stimulus (n = 12 fish) in 10-min bins over a 24-h period, showing mean seconds of activity per bin (bold) ± s.e.m. (shaded). Bottom, sleep depicted as minutes of sleep per 10-min bin (bold) ± s.e.m. (shaded) across the 24-h period. The black triangle depicts the day-tonight transition, the white triangle depicts the night-to-day transition and the orange triangle shows the time of feeding. **c**, **d**, fPSG recording of SBS (**c**) and PWS (**d**) during normal night phase. Red box shows transient synchrony in dorsal pallium, indicative of SBS. Activity traces from fEOG (top), fEEG (middle) and fEMG (bottom). fEEG and fEMG are $\Delta F/F$ traces from 14 masks

covering broad brain regions (as labelled), with integration of neuronal activity across 1-s bins. See Supplementary Information for reproducibility information.

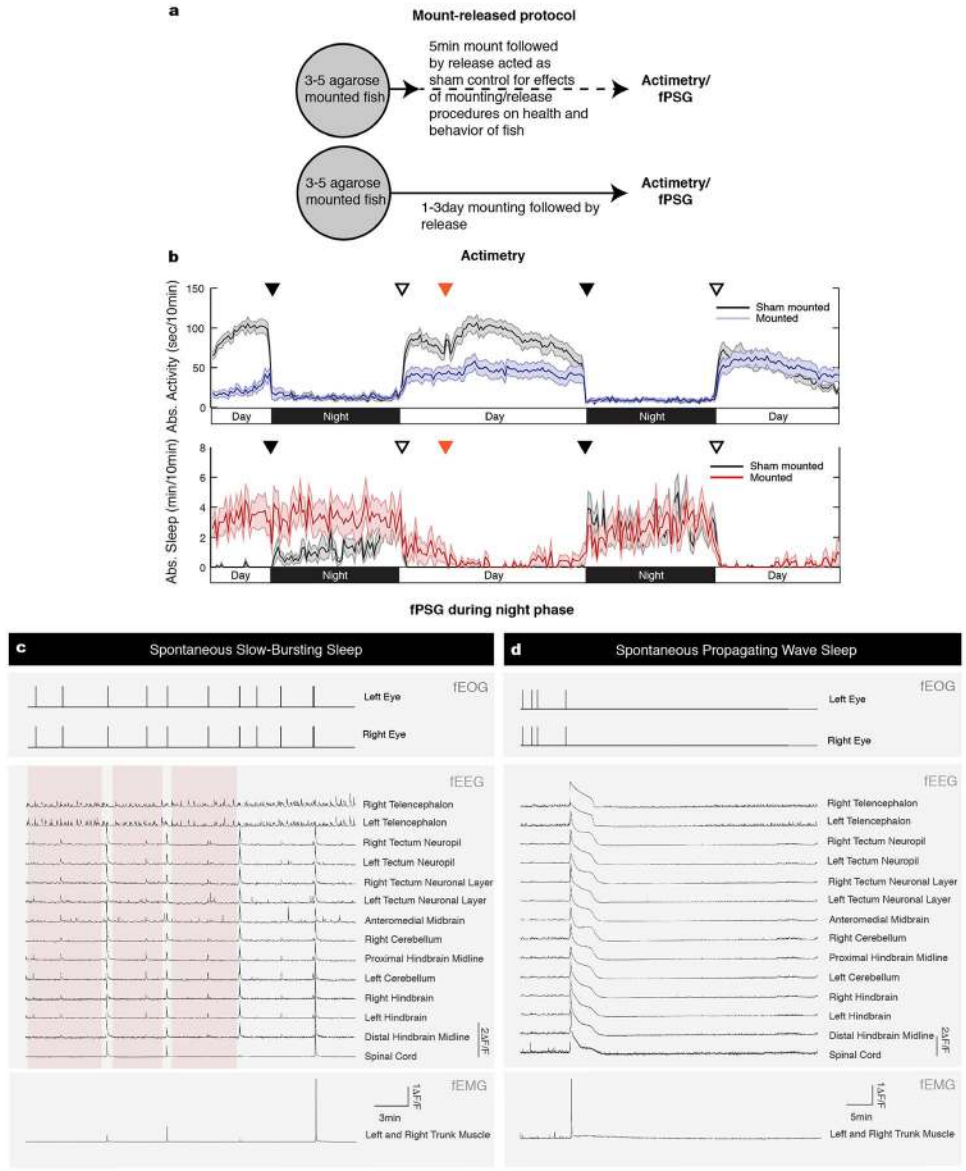

Extended Data Fig. 11 |. SPIM imaging reveals spontaneous SBS and PWS during the night phase.

a, Schematic of protocol to sham mount versus extended agarose mount for 1–3 days to test the degree of wake stimulation resulting from agarose restraint. **b**, Behavioural actimetry shows that while initially agarose-mounted animals display sleep behaviour upon release, sleep–wake cycles return to normal; this indicates that long-term restraint is not traumatic or lethal to zebrafish larvae. Actimetry of sham-mounted ($n = 36$ fish) versus mounted ($n = 31$ fish) wild-type zebrafish, in 10-min bins over a 24-h period showing mean seconds of activity per bin (bold) ± s.e.m. (shaded). Bottom, sleep depicted as minutes of sleep per 10-min bin (bold) ± s.e.m. (shaded), across the 24-h period. The black triangles depict the day-to-night transition, the white triangles depict the night-to-day transition and the orange triangle shows the time of feeding. **c**, **d**, fPSG recording of SBS(**c**) and PWS (**d**) during normal night phase. Red box shows transient synchrony in dorsal pallium, indicative of SBS

between muscle twitches. Activity traces from fEOG (top), fEEG (middle) and fEMG (bottom). fEEG and fEMG are $\Delta F/F$ traces from 14 masks covering broad brain regions (as labelled), with integration of neuronal activity across 1-s bins. See Supplementary Information for reproducibility information.

Acknowledgements

We thank all members of the Mourrain laboratory for helpful feedback and discussion during the project and preparation of the manuscript; L. de Lecea, J. Zeitzer, C. Heller, D. Grahn, D. Colas and A. Adamantidis for important feedback; P. Raymond, K. Kwan and H. Burgess for sharing constructs and lines; S. Nishino for the kind gift of zolpidem; L. Alexandre and S. Murphy for their diligent care of our zebrafish; Stanford Cell Sciences Imaging Facility for imaging assistance (funded by NCRR award S10RR02557401); and J. Goldberg (Research To Prevent Blindness) and Stanford Vision Research Core (NIH P30-EY0268771). Funding support was provided by Stanford School of Medicine Dean's fellowship (L.C.L.); JP18H04988, NBRP from AMED (K.K.); NIMH, NIDA, DARPA, NSF, Wiegers Family Fund, AE Foundation, Tarlton Foundation, and Gatsby Foundation (K.D.); NIMH, NINDS, Tashia and John Morgridge Fund (A.E.U.); and NIDDK (5R01DK090065-05), NINDS, NIMH, NIA, Bright-Focus Foundation, Simons Foundation and John Merck Fund (P.M.).

References

1. Campbell SS & Tobler I Animal sleep: a review of sleep duration across phylogeny. Neurosci. Biobehav. Rev 8, 269–300 (1984). [PubMed: 6504414]
2. Leung LC & Mourrain P Sleep: short sleepers should keep count of their hypocretin neurons. Curr. Biol 28, R558–R560 (2018). [PubMed: 29738730]
3. Pieron H Le Probleme Physiologique su Sommeil (Masson, 1913).
4. Shein-Idelson M, Ondracek JM, Liaw HP, Reiter S & Laurent G Slow waves, sharp waves, ripples, and REM in sleeping dragons. Science 352, 590–595 (2016). [PubMed: 27126045]
5. Prober DA et al. Hypocretin/orexin overexpression induces an insomnia-like phenotype in zebrafish. J. Neurosci 26, 13400–13410 (2006). [PubMed: 17182791]
6. Yokogawa T et al. Characterization of sleep in zebrafish and insomnia in hypocretin receptor mutants. PLoS Biol. 5, e277 (2007). [PubMed: 17941721]
7. Zhdanova IV Sleep in zebrafish. Zebrafish 3, 215–226 (2006). [PubMed: 18248262]
8. Aho V et al. Homeostatic response to sleep/rest deprivation by constant water flow in larval zebrafish in both dark and light conditions. J. Sleep Res 26, 394–400 (2017). [PubMed: 28251715]
9. Appelbaum L et al. Sleep-wake regulation and hypocretin-melatonin interaction in zebrafish. Proc. Natl Acad. Sci. USA 106, 21942–21947 (2009). [PubMed: 19966231]
10. Mueller T, Dong Z, Berberoglu MA & Guo S The dorsal pallium in zebrafish, *Danio rerio* (Cyprinidae, Teleostei). Brain Res. 1381, 95–105 (2011). [PubMed: 21219890]
11. Berman JR, Skariah G, Maro GS, Mignot E & Mourrain P Characterization of two melanin-concentrating hormone genes in zebrafish reveals evolutionary and physiological links with the mammalian MCH system. J. Comp. Neurol 517, 695–710 (2009). [PubMed: 19827161]
12. Chen TW et al. Ultrasensitive fluorescent proteins for imaging neuronal activity. Nature 499, 295–300 (2013). [PubMed: 23868258]
13. Madelaine R et al. MicroRNA-9 couples brain neurogenesis and angiogenesis. Cell Reports 20, 1533–1542 (2017). [PubMed: 28813666]
14. Chauvette S, Crochet S, Volgushev M & Timofeev I Properties of slow oscillation during slow-wave sleep and anesthesia in cats. J. Neurosci 31, 14998–15008 (2011). [PubMed: 22016533]
15. Borbély AA A two process model of sleep regulation. Hum. Neurobiol 1, 195–204 (1982). [PubMed: 7185792]
16. Borbély AA, Daan S, Wirz-Justice A & Deboer T The two-process model of sleep regulation: a reappraisal. J. Sleep Res 25, 131–143 (2016). [PubMed: 26762182]
17. Ikeda-Sagara M et al. Induction of prolonged, continuous slow-wave sleep by blocking cerebral H_1 histamine receptors in rats. Br. J. Pharmacol 165, 167–182 (2012). [PubMed: 21699505]

18. Marzanatti M, Monopoli A, Trampus M & Ongini E Effects of nonsedating histamine H1-antagonists on EEG activity and behavior in the cat. Pharmacol. Biochem. Behav 32, 861–866 (1989). [PubMed: 2572005]
19. Saitou K, Kaneko Y, Sugimoto Y, Chen Z & Kamei C Slow wave sleep-inducing effects of first generation H1-antagonists. Biol. Pharm. Bull 22, 1079–1082 (1999). [PubMed: 10549859]
20. Niethard N et al. Sleep-stage-specific regulation of cortical excitation and inhibition. Curr. Biol 26, 2739–2749 (2016). [PubMed: 27693142]
21. Dissel S et al. Sleep restores behavioral plasticity to *Drosophila* mutants. Curr. Biol 25, 1270–1281 (2015). [PubMed: 25913403]
22. Che Has AT et al. Zolpidem is a potent stoichiometry-selective modulator of α1β3 $GABA_A$ receptors: evidence of a novel benzodiazepine site in the α1–α1 interface. Sci. Rep 6, 28674 (2016). [PubMed: 27346730]
23. Sitaram N, Wyatt RJ, Dawson S & Gillin JC REM sleep induction by physostigmine infusion during sleep. Science 191, 1281–1283 (1976). [PubMed: 176724]
24. Callaway CW, Lydic R, Baghdoyan HA & Hobson JA Pontogeniculooccipital waves: spontaneous visual system activity during rapid eye movement sleep. Cell. Mol. Neurobiol 7, 105–149 (1987). [PubMed: 3308096]
25. Datta S Cellular basis of pontine ponto-geniculo-occipital wave generation and modulation. Cell. Mol. Neurobiol 17, 341–365 (1997). [PubMed: 9187490]
26. Baghdoyan HA, Lydic R, Callaway CW & Hobson JA The carbachol-induced enhancement of desynchronized sleep signs is dose dependent and antagonized by centrally administered atropine. Neuropsychopharmacology 2, 67–79 (1989). [PubMed: 2572234]
27. Coleman CG, Lydic R & Baghdoyan HA M2 muscarinic receptors in pontine reticular formation of C57BL/6J mouse contribute to rapid eye movement sleep generation. Neuroscience 126, 821–830 (2004). [PubMed: 15207317]
28. Datta S, Quattrochi JJ & Hobson JA Effect of specific muscarinic M2 receptor antagonist on carbachol induced long-term REM sleep. Sleep 16, 8–14 (1993). [PubMed: 8456236]
29. Árnason BB, Þorsteinsson H & Karlsson KAE Absence of rapid eye movements during sleep in adult zebrafish. Behav. Brain Res 291, 189–194 (2015). [PubMed: 26003945]
30. Roessmann U, Velasco ME, Sindely SD & Gambetti P Glial fibrillary acidic protein (GFAP) in ependymal cells during development. An immunocytochemical study. Brain Res. 200, 13–21 (1980). [PubMed: 6998542]
31. Conductier G et al. Control of ventricular ciliary beating by the melanin concentrating hormone-expressing neurons of the lateral hypothalamus: a functional imaging survey. Front. Endocrinol 4, 182 (2013).
32. Dale N Purinergic signaling in hypothalamic tanycytes: potential roles in chemosensing. Semin. Cell Dev. Biol 22, 237–244 (2011). [PubMed: 21396904]
33. Rizzoti K & Lovell-Badge R Pivotal role of median eminence tanycytes for hypothalamic function and neurogenesis. Mol. Cell. Endocrinol 445, 7–13 (2017). [PubMed: 27530416]
34. Peyron C, Sapin E, Leger L, Luppi PH & Fort P Role of the melanin-concentrating hormone neuropeptide in sleep regulation. Peptides 30, 2052–2059 (2009). [PubMed: 19660508]
35. Logan DW, Burn SF & Jackson IJ Regulation of pigmentation in zebrafish melanophores. Pigment Cell Res. 19, 206–213 (2006). [PubMed: 16704454]
36. Torterolo P, Lagos P, Sampogna S & Chase MH Melanin-concentrating hormone (MCH) immunoreactivity in non-neuronal cells within the raphe nuclei and subventricular region of the brainstem of the cat. Brain Res. 1210, 163–178 (2008). [PubMed: 18410908]
37. Conductier G et al. Melanin-concentrating hormone regulates beat frequency of ependymal cilia and ventricular volume. Nat. Neurosci 16, 845–847 (2013). [PubMed: 23708141]
38. Hassani OK, Lee MG & Jones BE Melanin-concentrating hormone neurons discharge in a reciprocal manner to orexin neurons across the sleep–wake cycle. Proc. Natl Acad. Sci. USA 106, 2418–2422 (2009). [PubMed: 19188611]
39. Jego S et al. Optogenetic identification of a rapid eye movement sleep modulatory circuit in the hypothalamus. Nat. Neurosci 16, 1637–1643 (2013). [PubMed: 24056699]

40. Kawauchi H, Kawazoe I, Tsubokawa M, Kishida M & Baker BI Characterization of melanin-concentrating hormone in chum salmon pituitaries. Nature 305, 321–323 (1983). [PubMed: 6621686]

41. Kwan KM et al. The Tol2kit: a multisite gateway-based construction kit for Tol2 transposon transgenesis constructs. Dev. Dyn 236, 3088–3099 (2007). [PubMed: 17937395]

42. Hieber V, Dai X, Foreman M & Goldman D Induction of α1-tubulin gene expression during development and regeneration of the fish central nervous system. J. Neurobiol 37, 429–440 (1998). [PubMed: 9828048]

43. Muto A, Ohkura M, Abe G, Nakai J & Kawakami K Real-time visualization of neuronal activity during perception. Curr. Biol 23, 307–311 (2013). [PubMed: 23375894]

44. Bernardos RL & Raymond PA GFAP transgenic zebrafish. Gene Expr. Patterns 6, 1007–1013 (2006). [PubMed: 16765104]

45. Tabor KM et al. Direct activation of the Mauthner cell by electric field pulses drives ultrarapid escape responses. J. Neurophysiol 112, 834–844 (2014). [PubMed: 24848468]

46. Appelbaum L et al. Circadian and homeostatic regulation of structural synaptic plasticity in hypocretin neurons. Neuron 68, 87–98 (2010). [PubMed: 20920793]

47. Renier C et al. Genomic and functional conservation of sedative-hypnotic targets in the zebrafish. Pharmacogenet. Genomics 17, 237–253 (2007). [PubMed: 17496723]

48. Rihel J et al. Zebrafish behavioral profiling links drugs to biological targets and rest/wake regulation. Science 327, 348–351 (2010). [PubMed: 20075256]

49. Pitrone PG et al. OpenSPIM: an open-access light-sheet microscopy platform. Nat. Methods 10, 598–599 (2013). [PubMed: 23749304]

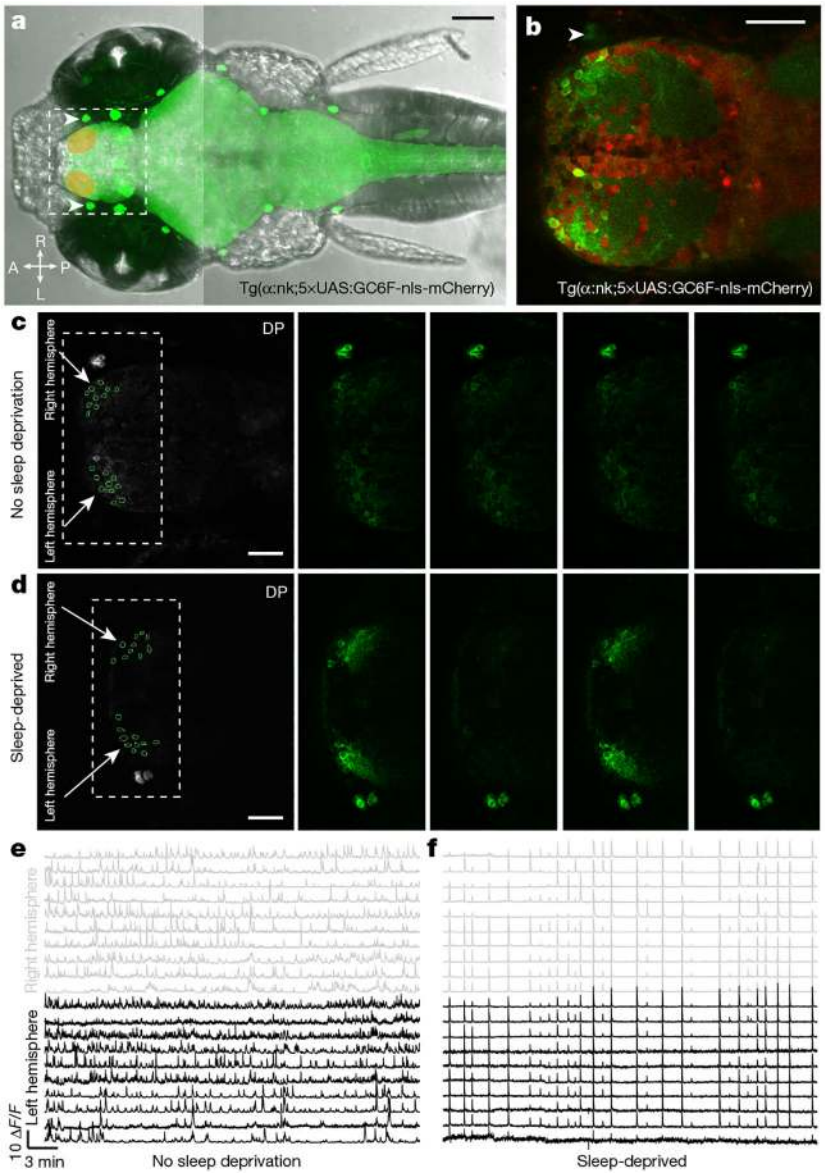

Fig. 1 |. Sleep deprivation produces slow bursting activity in the zebrafish dorsal pallium.

a, Dorsal view of a brain from Tg(a:nk;5×UAS:GCaMP6F-p2a-nls-mCherry) (see Methods for details of zebrafish lines) zebrafish at seven days post-fertilization (only GCaMP is shown), superimposed on its body plan (transmitted light). Orange ovals depict anterolateral dorsal pallium, at which high spontaneous awake activity occurs. Scale bar, 100 μm. A, anterior; L, left; R, right; P, posterior. **b**, Single *z*-slice image of the telencephalic region (GCaMP (green) and nuclear-localized mCherry (red)) from dashed box in **a**, at the level of the neuromast fiduciary marker (white arrowhead). Scale bar, 50 μm. **c**, **d**, Left, representative images showing 20 masks on non-sleep-deprived (**c**) or sleep-deprived (**d**) brains. Right, magnified clips of Ca^{2+} imaging in the dorsal pallium (DP) from the region in dashed box in the leftmost panel. Scale bars, 50 μm. **e**, **f**, Time-aligned $\Delta F/F$ traces of the 20 neurons from non-sleep-deprived fish (**e**) marked in **c** and sleep-deprived fish(**f**) marked in **d**. Desynchronous versus synchronous indices, ITI: 3.84 ± 0.14 s versus 12.26 ± 2.91 s; P=

0.00018, Wilcoxon rank-sum test $n = 10$ fish per condition; coherence index, 6.32% ($n =$ 40,175 spikes) versus 18.84% ($n = 41{,}161$ spikes); $P < 0.05$, χ^2 test.

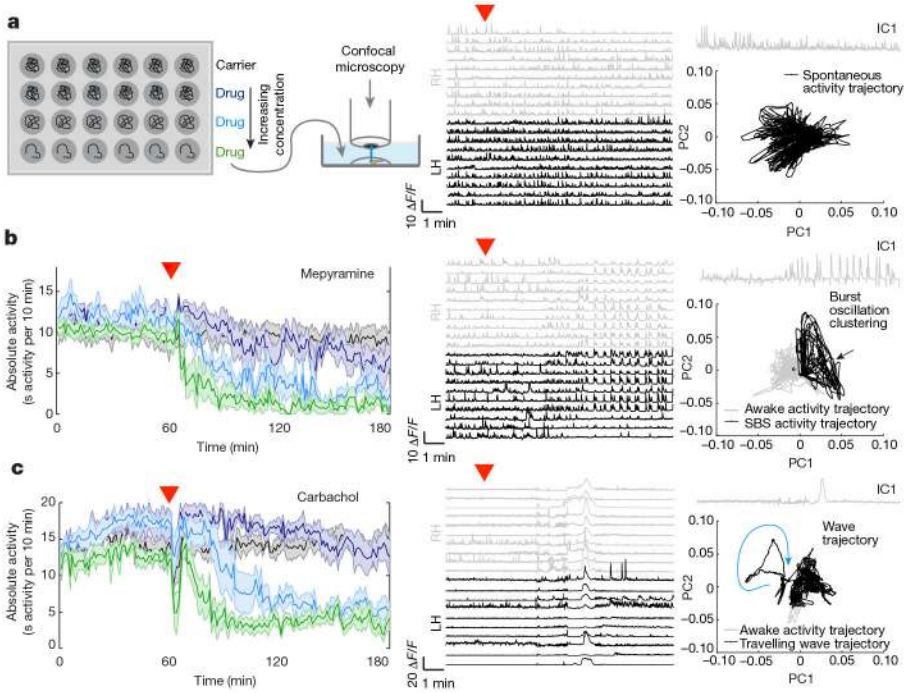

Fig. 2 |. Hypnotics induce heterogeneous effects on telencephalic activity.

a, Left, schematic of experimental pipeline. Compounds are first validated as hypnotic by screening freely behaving fish, before being applied to agar-restrained fish for Ca^{2+} imaging. Middle, time-aligned $\Delta F/F$ traces of 20 randomly selected dorsal pallium neurons from a carrier-stimulated fish (red triangle indicates addition after 10 min). Right, neural signature across all time points represented by the first independent component (IC) (top) or replotted following principal components analysis (PCA) (bottom). LH, left hemisphere; RH, right hemisphere. **b**, **c**, Left, three-hour actimetry recordings, in which a range of drug dosages were added after one hour (red triangle). Activity traces are expressed as the number of seconds active per ten-minute time bin, and plotted as trial-averaged mean (solid line) ± s.e.m. (shaded) per dose of mepyramine (**b**, $n = 24$ fish), and carbachol (**c**, $n = 24$ fish) from low to high (black < purple < blue < green; see Supplementary Table 1 for concentrations), showing induction of dose-responsive behavioural sleep. Middle and right plots show representative time-aligned $\Delta F/F$ traces, independent component analysis and PCA (grey and black lines depict wake and sleep dynamics, respectively) for respective drugs. Wake versus mepyramine SBS synchronicity indices: ITI, 4.42 ± 0.38 s versus 16.55 ± 6.79 s, $P = 0.041$, Wilcoxon rank-sum test, $n = 6$fish and coherence index 6.06% ($n = 5{,}177$ spikes) versus 31.18% ($n = 7{,}215$ spikes), $P < 0.00001$, χ^2 test. See Supplementary Information for reproducibility information.

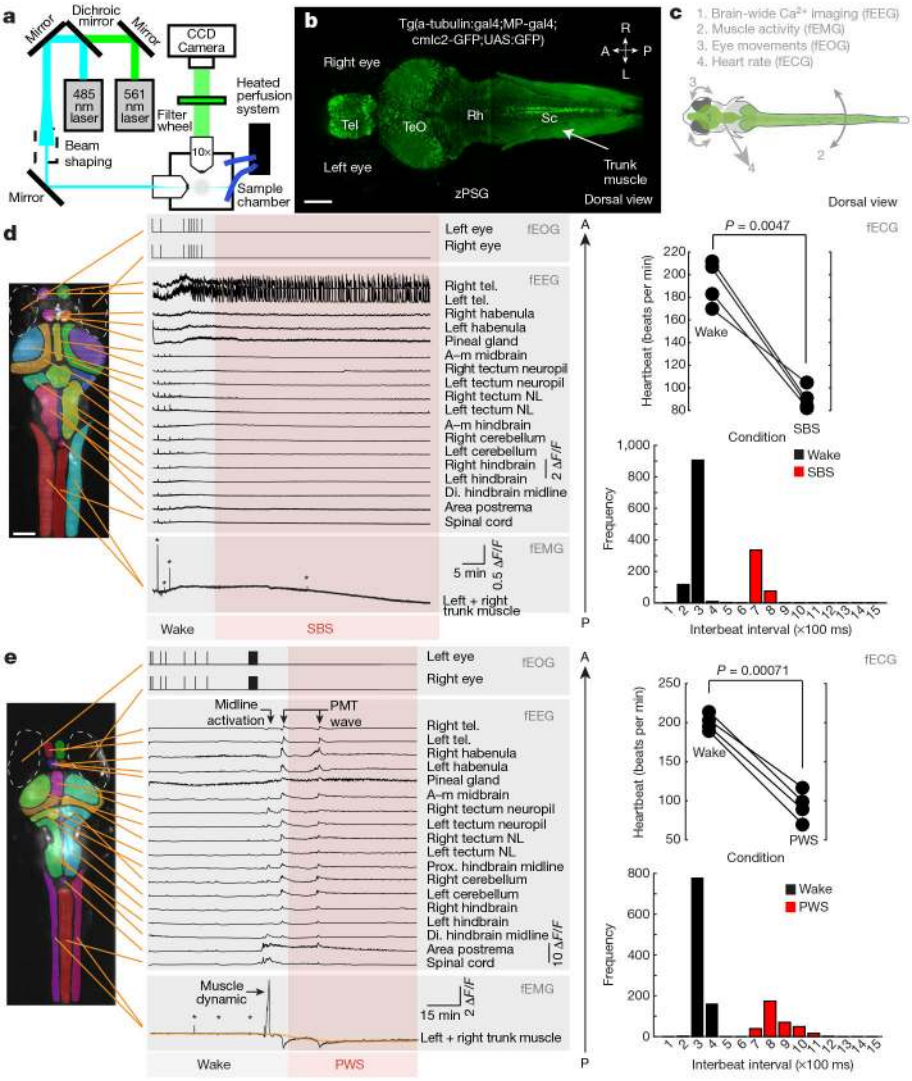

Fig. 3 |. Fluorescence-based polysomnography reveals SBS and PWS in zebrafish.

a, Schematic diagram of the light-sheet microscope platform (based on the openSPIM design; see 'fPSG' in 'Sample preparation and Ca^{2+} imaging' in Methods) used to take time-lapse recordings of synchronous *x*–*y* frames as single slices or volumes customized with temperature control and drug perfusion apparatus. **b**, Single *z*-plane (dorsal view) of a zPSG transgenic fish at seven days post-fertilization, co-expressing a trunk muscle gal4 and pan-neuronal gal4 used to drive expression of UAS:GCaMP7a. Broad brain regions are indicated as telencephalon (Tel), optic tectum (TeO), rhombencephalon (Rh) and spinal cord (Sc). Scale bar, 100 μm. **c**, Depiction of parameters that can be measured, based on fluorescent markers of zPSG fish that form an fPSG. **d**, **e**, Left, broad fPSG region-of-interest masks on a maximum projection image to measure GCaMP activity before, during and after initiation of SBS (**d**) or PWS (**e**). Middle, Brain and muscle activity traces ($\Delta F/F$) from broad regions defined by masks (middle panels show fEEG and bottom panels show fEMG), with integration of activity across 1 s (**d**) or 2.5 s (**e**) bins. Asterisks denote muscle contractions. Time trace of eye movements (fEOG) is shown in the top panels. Right, heart rate (fECG),

measured before and after recording of SBS (**d**) or PMT wave (**e**) (top), and distribution of interbeat intervals (bottom). $*P < 0.05$. Two-sided paired *t*-test, $n = 4$ fish per condition. A–m, anteromedial; di., distal; NL, neuronal layer; prox., proximal.

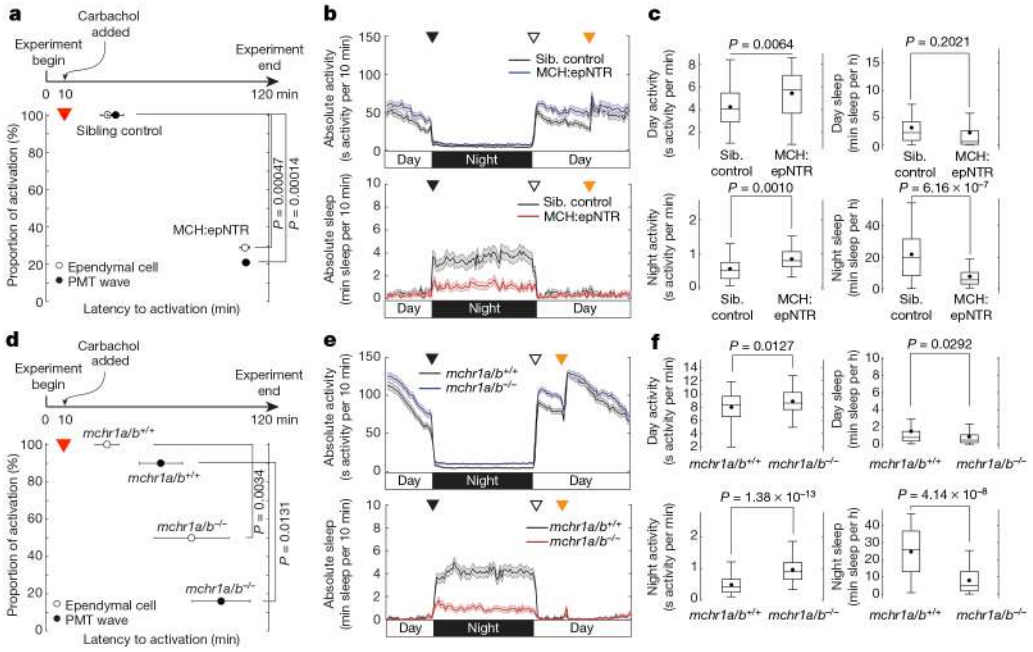

Fig. 4 |. MCH signalling is required for sleep and generation of PWS dynamics.

a–**f**, MCH2 neuron-ablated (**a**–**c**) and MCHR mutant (**d**–**f**) fish display increased activity, decreased sleep and disrupted onset of ependymal cell and PMT-wave dynamics. **a**, **d**, Top, timeline of a two-hour Ca^{2+} imaging experiment with addition of the PWS inducer (red triangle). Bottom, proportion of sibling (sib.)-treated control ($n = 10$ fish) versus MCH2-ablated ($n = 14$ fish) groups (**a**) or *mchr1a*$^{+/+}$*mchr1b*$^{+/+}$ (*mchr1a/b*$^{+/+}$) controls ($n = 10$ fish) versus *mchr1a*$^{-/-}$*mchr1b*$^{-/-}$ (*mchr1a/b*$^{-/-}$) double mutants ($n = 6$ fish) (**d**) with ependymal (open circle) and/or PMT-wave (filled circle) activation within the imaging session, plotted against the mean latency to activation (min) ± s.e.m. *$P < 0.05$ χ^2 test. **b**, **e**, Top, actimetry of sibling-treated control ($n = 42$) versus MCH2-neuron-ablated ($n = 44$) fish (**b**) or *mchr1a*$^{+/+}$*mchr1b*$^{+/+}$ ($n = 67$) versus *mchr1a*$^{-/-}$*mchr1b*$^{-/-}$ double mutant ($n = 72$) fish (**e**) in 10-min bins over a 24-h period, showing mean seconds of activity per bin (bold) ± s.e.m. (shaded). Bottom, sleep depicted as minutes per 10-min bin ± s.e.m. (shaded). Black or white triangles indicate day-to-night or night-to-day transitions, respectively, and orange triangles show time of feeding. **c**, **f**, Box plots showing spread of total activities and sleep between sibling-treated control versus MCH2-neuron-ablated (**c**) or *mchr1a*$^{+/+}$*mchr1b*$^{+/+}$ versus *mchr1a*$^{-/-}$*mchr1b*$^{-/-}$ double (**f**) groups separated out by day and night. Blue lines and black circles denote the median and mean, respectively. Two-sided Student's *t*-test.